Original Article

The Effect of Zinc Oxide Nanoparticles and Their Withdrawal on the Pancreatic Acini of Adult Male Albino Rats: A Histological, Biochemical and Morphometric Study

Reham Said Ahmed Mahmoud Zaghloul, Mostafa Mahmoud Abo El Ela, Safaa Gomaa Takey El Din and Silvia Kamil Seddik Sawires

Department of Histology and Cell Biology, Faculty of Medicine, University of Alexandria, Egypt

ABSTRACT

Introduction: Zinc oxide nanoparticles (ZnO-NPs) are one of metal nanoparticles that have broadly utilized in numerous fields. Nowadays, they are increasingly utilized in food as a preservative. Therefore, humans become more susceptible to their hazards via oral route.

Objective: To assess the impact of different doses of ZnO-NPs on the pancreatic acini and the effect of their withdrawal.

Materials and Methods: Thirty adult male albino rats were distributed into three equal groups at random. Group I acted as control. Group II (ZnO-NPs treated group): subdivided into two subgroups received ZnO-NPs in doses of 100 and 400 mg/kg body weight/day respectively for 28 days by oral gavage. Group III (withdrawal group): subdivided into two subgroups administered ZnO-NPs as in group II then left for 1 month without treatment. At the designated time, blood samples were collected for biochemical analysis. After scarification, pancreatic tissue was obtained and managed for light and electron microscopic studies. All the gained data underwent statistical analysis.

Results: ZnO-NPs treated group showed dose-dependent pancreatic acinar cell damage. The cells exhibited vacuolations, rarefaction, dilated rough endoplasmic reticulum, nuclear condensation and mitochondrial degeneration which were more apparent in high doses. Moreover, biochemical studies showed a statistically significant rise in pancreatic and oxidant markers. In addition, morphometrical analysis revealed a statistically significant increase in area percentage of collagen deposition. However, ZnO-NPs withdrawal induced a great recovery concerning 100mg-treated rats but incomplete improvement was detected in 400mg-treated rats.

Conclusion: ZnO-NPs induce structural and functional alterations on the pancreatic acini which are dose- dependent. When ZnO-NPs were withdrawn, these changes were reversible at low doses but partially improved with high doses.

Received: 06 September 2022, **Accepted:** 04 October 2022

Key Words: Microscopic examination, pancreatic acini, withdrawal, zinc oxide nanoparticles.

Corresponding Author: Silvia Kamil Seddik Sawires, PhD, Department of Histology and Cell Biology, Faculty of Medicine, University of Alexandria, Egypt, **Tel.**: +20 12 2695 0510, **E-mail:** silviakamil76@yahoo.com

ISSN: 1110-0559, Vol. 46, No. 4

INTRODUCTION

One of the significant breakthroughs of the twenty-first century that is undergoing rapid expansion is nanotechnology[1]. It is the science and engineering that goes into designing, synthesizing, characterizing, and using materials at the nanoscale scale (one nanometer is equal to one-billionth of a meter)[2]. Public interest in nanotechnology has increased significantly as a result of the widespread use of nanomaterials in commerce, industry, agriculture, medicine, and public health[3,4].

A special attention to risk assessment is required in light of the expanding use of commercial products based on engineered nanoparticles (NPs), with the purpose of developing safer nanomaterials[5]. Their wide use in different industries can lead to an environmental contamination and human health problems. Moreover, NPs application in biomedical fields involves direct human exposure[6,7].

Among the most interesting and promising metallic nanomaterials are zinc oxide nanoparticles (ZnO-NPs). They are considered a multifunctional material owing to their distinctive physical, chemical, optical and electrical characteristics such as: conductivity, high refractive index, high chemical stability, high photostability, UV protection and antibacterial capabilities[8,9]. Therefore, they have a wide application in various products and materials, including: cosmetics, medicine, solar cells, paints, rubber and concrete[10,11]. Besides, ZnO-NPs have strong photocatalytic properties for organic contaminants in water and are employed as food additives and in food packaging[12].

A contentious dispute over ZnO-NPs' effects on human health has arisen as a result of the inescapable exposure to these particles[13]. Due to their diminutive size, ZnO-NPs may be more readily inhaled and absorbed by people through their airways, occasionally through their digestive tracts or skin[14].

 DOI: 10.21608/ejh.2022.161063.1765

According to experimental research on animals, oral exposure to ZnO- NPs in rats caused toxicity in the kidney, liver, pancreas, heart, and bone[15,16]. Similar to this, rats given ZnO-NPs by gavage experienced negative alterations in their hematological indices, histological changes in their spleen, stomach, brain, pancreas, as well as genotoxicity[17,18].

Concerning the pancreas, many studies proved that oral administration of ZnO-NPs resulted in significant antidiabetic effects on islets of Langerhans,[19-22] which makes it important to investigate their effect on the neighboring pancreatic acinar cells. Till recently, the majority of in *vivo* histological research on ZnO-NPs toxicity has concentrated on evaluating acute toxicity or repeated-dose toxicity via various routes[17,23]. Only few researchers investigated a prolonged exposure toxicity[24,25].

In view of the previously mentioned facts, it has become quite indispensible to inspect the possible histological and biochemical changes produced by different doses of ZnO-NPs on the pancreatic acini, to estimate the degree of the cellular response to them in-*vivo*. Moreover, the study was further extended for one month, to investigate the possible spontaneous recovery on cessation of administration of ZnO-NPs.

MATERIALS AND METHODS

Chemical

Zinc oxide nanoparticles (average size 20 nm), in the form of white powder, were obtained from Nanotech Egypt for Photo-Electronics Company (City of 6 October, Egypt). Every day, a new batch of suspension was made (just before the administration). Zinc oxide nanoparticles were dissolved in distilled water, sonicated for 10-15 minutes using USR3/2907 sonicator (JulaboLabortechnik, Seelbach, Germany) and mechanically vibrated for 2-3 minutes to increase the dispersion of the particles and thereby diminish clumping[26].

Characterization of the zinc oxide nanoparticles

1- Transmission electron microscope (TEM)

The morphology and size of the NPs employed were assessed by Jeol 1400 plus electron microscope (Tokyo, Japan) at the Electron Microscopy Unit, Faculty of Science, Alexandria University[9].

2- Nano Zeta particle analyzer

The exact size and zeta potential (surface charge) of the NPs were evaluated using a Nano Zeta sizer particle analyzer {(Malvern, UK), Central Lab, Faculty of Pharmacy, Alexandria University}[27].

3- X-ray diffraction (XRD)

X-ray diffraction (XRD) is utilized for characterizing the crystal structures[9]. ZnO NPs' powder was analyzed by X-ray diffracto-meter {(Shimadzu XRD-7000, Maxima, Japan), City of Scientific Research and Technological Applications, Borg El Arab}. The voltage and current used were 30 kilovolts and 30 milliampere respectively

4- Ultraviolet-visible absorption spectroscopy

Ultraviolet-visible (UV-Vis) analysis was carried out on a dual beam spectroscopy {(UNICAM UV-Vis spectrometry model UV5-220), Medical Biophysics Department, Medical Research Institute, University of Alexandria}, using deionized water as the reference. The Surface Plasmon Resonance of the NPs was indicated by their UV-Vis spectrum[9].

Experimental animals

A total of 30 adult male Sprague Dawley albino rats were involved in this study, with an average weight of ~200 gm. The animals were 6-8 weeks old, gained from the animal house of the Medical Research Institute, Alexandria University. Before the experiment, the animals were given a two-week acclimation period. They were kept under conventional laboratory conditions, which included temperature, humidity, and a 12-hour light/dark cycle. All techniques were permitted by the Local Ethics Committee of the Faculty of Medicine, Alexandria University IRB number 00012098.

The rats were categorized into 3 main groups at random. All animals were received treatment through oral gavage.

Group I (control group): consisted of ten rats divided into two equal subgroups;

- Subgroup IA: got no treatment.
- Subgroup IB: each rat was given distilled water of 10ml/kg body weight day[28].

Group II (ZnO-NPs treated group): 10 rats were subdivided into two equal subgroups, each animal received ZnO-NPs once daily for 28 days[29]:

- Subgroup IIA: was given ZnO-NPs in a dose of 100 mg/kg body weight/day[28].
- Subgroup IIB: received ZnO-NPs in a dose of 400 mg/kg body weight/day[28].

Group III (withdrawal group):10 rats were subdivided into two equal subgroups (subgroup IIIA and IIIB) administered ZnO-NPs as in group II then left for 1 month without treatment for spontaneous recovery

Sampling

At the end of the research, animals were anesthetized by intraperitoneal injection of Ketamine (90mg/kg)[30]. For biochemical analysis, 4ml of blood from each rat's retro-orbital plexus were collected with capillary glass tubes. The samples were centrifuged at 1000 x g for 15 min, the sera were separated, and the samples were kept at -20 oC. After scarification, the pancreas of each albino rat was dissected out carefully and prepared for histological study.

Biochemical study

Measurement of pancreatic Malondialdehyde (MDA)

MDA concentrations were assessed as indicators of oxidative stress. Pancreatic tissue was crushed, homogenized in 10% phosphate-buffered saline (PBS) and then sonicated in order to prepare it for MDA assessment. To remove debris and nuclei, the homogenate was centrifuged for 5 minutes at 10,000 rpm (-4 °C). MDA level was estimated directly from the supernatant. The MDA calorimetric test offers a precise method for MDA detection using a Humalyzer junior photometer (Human Diagnostics, Germany) at the Biochemistry Department, University of Alexandria, Egypt. Thiobarbituric acid (TBA) and MDA in the sample interact to form the MDA-TBA adduct, which is measurable and quantifiable colorimetrically (OD= 532 nm)[31].

Measurement of serum levels of pancreatic lipase and amylase

Using commercial kits and a Roche/Hitachi modular analytics system (Roche, Mannheim, Germany) at the Biochemistry Department, University of Alexandria, Egypt, the serum levels of amylase and lipase were determined utilizing enzyme dynamics chemistry in accordance with the manufacturer's instructions[32].

Histological study

A part of the pancreatic tissue was obtained from the animals of all groups was fixed in 10% formol saline and handled to get 6 μm thick paraffin sections. These sections were stained with hematoxylin and eosin (H&E) stain for morphological study[33] and Gomori's trichrome stain[33] to study the collagen distribution and viewed under the light microscope (Olympus, Japan) supplied with a digital camera (Olympus, Japan) at the Center of Excellence for Research in Regenerative Medicine and its Applications (CERRMA), Alexandria Faculty of Medicine.

Another part of the pancreatic tissue was promptly cut into tiny cubes (0.5-1 mm3), fixed at 4°C in phosphate buffered glutaraldehyde at a 3 percent concentration, and then post-fixed for 1-2 hours in osmium tetroxide at a 1 percent concentration. The samples were then embedded in epon after being dehydrated with graded ethanol[34]. Semithin sections were acquired, stained with toluidine blue stain and viewed under the light microscope using the oil immersion lens at CERRMA (Olympus Tokyo, Japan, BX41).Ultrathin sections (80 nm thick) were made, placed on copper grids, and stained using lead citrate and uranyl acetate[35]. The grids were studied and photographed by TEM {(JEOL JEM-2100, Tokyo, Japan), Electron Microscopy Unit, Faculty of Agriculture, University of Mansoura and Electron Microscopy Unit, Faculty of Science, University of Alexandria}.

Quantitative morphometric study

The NIH Fiji software (NIH, Bethesda, USA) was utilized to estimate area percentage of collagen from images captured from Gomori's trichrome stained slides at microscopic magnification of 100. Measurements were gathered from five different fields of each animal at random. The gained data were presented as mean ± standard deviation (SD).

IV- Statistical analysis

The acquired data (including area percentage of collagen, mean values of pancreatic MDA, serum amylase and lipase levels) were fed into a computer, analyzed with IBM SPSS software version 20.0. (Armonk, NY: IBM Corp) and expressed as a mean + SD. To ascertain the statistical significance, one-way analysis of variance (ANOVA) and the "Tuckey" post-hoc test were utilized ($P < 0.05$ was considered significant).

RESULTS

Characterization of the zinc oxide nanoparticles

Transmission electron microscope (TEM)

The morphology and size of ZnO-NPs in the current research exhibited that individual particles have an average diameter of 11± 6 nm. They mostly consisted of nanorods with few spherical in shape, electron dense and made aggregates of various sizes (Figure 1).

Nano Zeta particle analyzer

The results depicted that the ZnO-NPs have zeta potential of -32 mv (Figures 2 a,b).

X-ray diffraction (XRD)

The XRD pattern of ZnO NPs conferred with data in the certificate of analysis got from Nanotech Egypt Chemical Company. The sharpness of the peak pattern in the XRD demonstrated a successful production of ZnO-NPs (Figure 3).

Ultraviolet-visible absorption spectroscopy

The prepared ZnO-NPs showed that UV-Vis absorption spectrum exhibited sharp absorption band in the UV region at ~370 nm, indicative of the formation of ZnO-NPs (Figure 4).

Biochemical results

Pancreatic Malondialdehyde (MDA)

Between the various control subgroups (IA and IB), the mean levels of pancreatic MDA did not show any statistically significant variation. ZnO-NPs administration caused a high statistically significant rise in pancreatic MDA levels in both subgroups IIA and IIB (doses of 100 and 400 mg/kg for 28 days respectively) compared to the control subgroups, with statistically significant increase in subgroup IIB compared to subgroup IIA. ZnO-NPs withdrawal resulted in a high statistically significant reduction of pancreatic MDA levels in subgroup IIIA (withdrawal dose of 100 mg/kg) as compared with subgroup IIA with no statistically significant difference compared to the control subgroups. In comparison to subgroup IIB, subgroup IIIB (withdrawal dose of 400 mg/kg) showed no statistically significant difference in the mean level of pancreatic MDA, with high statistically significant increase

when compared to the control subgroups and subgroup IIIA (Histogram 1a).

Serum lipase and amylase

ZnO-NPs administration at low and high doses resulted in a statistically significant rise in serum levels of both lipase and amylase enzymes in subgroups IIA and IIB (doses of 100 and 400 mg/kg for 28 days respectively) in comparison to the control subgroups (IA, IB) which showed no statistically significant difference among them. A statistically significant reduction in the serum levels of both enzymes was noticed in subgroup IIIA (withdrawal dose of 100 mg/kg) as compared with subgroup IIA with no statistically significant difference compared to the control subgroups. On the other hand, subgroup IIIB (withdrawal dose of 400 mg/kg) exhibited no statistically significant difference in comparison to subgroup IIB, with a high statistically significant increase as compared with the control subgroups and subgroup IIIA (Histogram 1 b,c).

Histological results

Haematoxylin and eosin results

Group I (control group): Light microscopic examination of sections of the pancreas of the control subgroups (IIA and IIB) revealed normal pattern of the pancreatic structure. The pancreatic acini were arranged in the form of lobules separated by narrow interlobular septa. The lining acinar cells were pyramidal in shape. The apical portion of the acinar cells revealed significant acidophilia, whereas the basal portion appeared basophilic. The nuclei of the acinar cells were mostly rounded, vesicular with apparent nucleoli. Interlobular ducts were seen in the sections. The endocrine portion of the pancreas appeared as pale acidophilic patches of islets of Langerhans, scattered among the pancreatic acini (Figures 5 a,b).

Group II (ZnO-NPs treated group):

Subgroup IIA (100 mg/kg for 28 days): Sections of the pancreas of the rats of this subgroup showed wide areas of normal acini. Other areas revealed cytoplasmic vacuolations in some acinar cells. Thickened interlobular septa and dilated interlobular ducts with flattening of their lining cells were seen, while the blood vessels showed dilatation and congestion. The dilated ducts and the congested blood vessels were surrounded by evident cellular infiltrate (Figures 6 a,b).

Subgroup IIB (400 mg/kg for 28 days): Examination of the exocrine pancreas of rats of this subgroup revealed that some acini appeared normal, while others showed prominent structural changes. Cytoplasmic vacuolations were found which sometimes were extensive up to the degree of cellular distortion. Some acinar cells exhibited hypereosinophilic cytoplasm. Some nuclei appeared vesicular with prominent nucleoli, while others were shrunken and pyknotic. In some areas, interlobular septa were thickened. Dilatation of the interlobular ducts together with flattening of the lining cells was observed. Evident periductal and perivascular cellular infiltration was noticed (Figures 6 c,d).

Group III (withdrawal group):

Subgroup IIIA (withdrawal dose of 100 mg/kg for 28 days): On examination of rats of this subgroup, restoration of the normal exocrine pancreatic architecture was revealed, where most of the acini were well organized into lobules. Most of the acinar cells showed the normal pattern of apical acidophilia and basal basophilia. Few acinar cells depicted small cytoplasmic vacuoles. Interlobular ducts were seen with normal appearance as the control group. On the other hand, widening of the interlobular septa was evident in some areas (Figures 7 a,b).

Subgroup IIIB (withdrawal dose of 400 mg/kg for 28 days): Studied pancreatic specimens of this subgroup revealed some normal acini, while some acinar cells showed cytoplasmic vacuolations. Shrunken pyknotic nuclei were detected as well as vesicular appearing ones with prominent nucleoli. Interlobular septa appeared widened. Dilated congested blood vessels were seen in thickened septa. Dilatation of some interlobular ducts with flattening of their lining cells was depicted. Marked periductal cellular infiltration was observed (Figures 7c,d).

Gomori's trichrome staining

Minimal amount of collagen fibers surrounding the blood vessels, the interlobular ducts and in the interlobular septa were seen in the control subgroups (IA, IB) (Figure 8a). Subgroup IIA (received 100 mg/kg ZnO-NPs for 28 days) depicted an increase in interlobular septa and perivascular collagen fibers (Figure 8b). Examination of the exocrine pancreas of rats of subgroup IIB (received 400 mg/kg ZnO-NPs for 28 days), revealed an apparent increase in collagen fibers in the interlobular septa and in between the acini. Increased collagen distribution in perivascular and periductal regions was evident (Figure 8c). Subgroup IIIA (withdrawal of dose 100mg/kg) showed almost normal pattern of collagen fibers' distribution. There was limited amount of peivascular and periductal collagen fibers (Figure 8d). Moderate increase in collagen fibers' distribution was noticed in the periductal and perivascular regions in subgroup IIIB (withdrawal of dose 400mg/kg) (Figure 8e).

Semithin section results

Inspection of semithin sections of the exocrine pancreas of the control subgroups displayed pancreatic acini lined by pyramidal cells with apical zymogen granules. The lumena of the acini were narrow and lined by flat pale staining centroacinar cells. Few acinar cells appeared binucleated. Intralobular ducts were seen lined by simple cuboidal epithelium (Figure 9a). Subgroup IIA (received ZnO-NPs 100 mg/kg for 28 days) revealed cytoplasmic vacuoles in some of the acinar cells. Some nuclei appeared with almost normal pattern, while others appeared small and deeply stained (Figure 9b). On examining semithin

sections of subgroup IIB (received ZnO-NPs 400 mg/kg for 28 days), several histological changes were observed, where most of the acini were seen with marked cytoplasmic vacuolations. Some nuclei appeared normal, whereas others appeared small with clumped chromatin. Dilated congested blood vessels were also detected (Figure 9c). In subgroup IIIA (withdrawal of dose 100mg/kg), semithin sections of the exocrine pancreas showed almost normal appearance, where the acini appeared well organized. Most of the nuclei had almost normal appearance. Intralobular ducts were realized lined by simple cuboidal epithelium (Figure 9d). Examination of semithin sections of the exocrine pancreas of subgroup IIIB (withdrawal of dose 400mg/kg) revealed cytoplasmic vacuoles in some acinar cells. Other acini were nearly devoid of vacuoles. Most of the nuclei seemed with almost normal chromatin pattern, while few nuclei showed condensed chromatin. Congested blood vessels were seen (Figure 9e).

Electron microscopic results

Group I (control group): Electron microscopic analysis of the ultrathin sections of the exocrine pancreas of rats of the control subgroups (IA, IB) exhibited normal appearance of the pancreatic acini. The pancreatic acini had narrow lamina that was surrounded by pyramidal shaped acinar cells. The apical portions of the cells were filled with electron dense membrane bounded zymogen granules. The basal portions of the cells were studded with rough endoplasmic reticulum with closely packed, flat and parallel cisternae. Mitochondria were also seen, in between divergent cisternae of the rough endoplasmic reticulum. The nuclei of the acinar cells were euchromatic, with regular outline and prominent nucleoli. Some acinar cells were binucleated. Centroacinar cells lining the lamina of the acini were apparent with their characteristic cytoplasm of low electron density and few organelles (Figure 10).

Group II (ZnO-NPs treated group):

Subgroup IIA (100 mg/kg for 28 days): On studying the ultrathin sections of the pancreas of rats of this subgroup showed many acini appeared normal, while others showed affection of their acinar cells. Some nuclei appeared regular with normal chromatin pattern and prominent nucleoli, while others were irregular with dilated perinuclear cisterna and chromatin condensation. In some acinar cells, the cisternae of rough endoplasmic reticulum appeared mildly dilated, while other cells exhibited normal cisternae. Few basal cytoplasmic vacuoles were noticed in some acinar cells. Some of the zymogen granules appeared with electron dense cores and surrounded by electron-lucent halos, some looked with very low electron density, while others revealed normal pattern. Fibroblasts and few collagen fibers were noticed in the interstitium between the acinar cells. Centroacinar cells were also seen (Figure 11).

Subgroup IIB (400 mg/kg for 28 days): The pancreas of this subgroup depicted significant ultrastructural changes affecting acinar cells. As regards the rough endoplasmic reticulum, marked dilatation, irregularity as well as discontinuation of its cisternae were seen. Nuclear changes of the acinar cells were also noticed. Some nuclei were regular and euchromatic, while others were irregular with clumping of their chromatin and dilatation of the perinuclear cisternae; others exhibited indistinct boundaries with interrupted nuclear envelope. Some cells exhibited degenerated mitochondria with apparent loss of cristae and decrease matrix density. In addition, noticeable areas of rarefaction of the cytoplasm were encountered in some pancreatic acinar cells. Considerable amount of collagen fibers' deposition was detected in the interstitium between the cells (Figure 12).

Group III (withdrawal group)

Subgroup IIIA (withdrawal dose of 100 mg/kg for 28 days): The rat pancreatic acini of this subgroup revealed almost normal pattern of pancreatic acinar cells. The pancreatic acini were lined by pyramidal shaped acinar cells. Apically situated zymogen granules were evident. Abundant cisternae of rER were seen with the normal appearance. Only few cells depicted mild dilated rER cisternae. Some cells showed few cytoplasmic vacuoles together with myelin figure like structures. Regarding the nuclei, most displayed regular outline, normal chromatin pattern and prominent nucleoli, while few displayed dilated perinuclear cisterna. Few amount of collagen fibers were sparsely distributed in the interstitium between the cells. (Figure 13)

Subgroup IIIB (withdrawal dose of 400 mg/kg for 28 days): Ultrathin sections of the exocrine pancreas of rats of this subgroup revealed moderate affection of pancreatic acinar cells. Some nuclei were euchromatic with apparent nucleoli, while others appeared with condensation of the chromatin and dilated perinuclear cisterna. In most of the cells, the rER was dilated and disorganized together with discontinuation of its cisternae. Some acinar cells revealed myelin figure like structures. In addition, collagen fibers were encountered in between the acini (Figure 14).

Quantitative morphometric study and statistical analysis of Area percentage of collagen

The mean area percentage of collagen was significantly increased in subgroups IIA, IIB and IIIB in comparison to the control subgroups (IA and IB) which showed no statistically significant difference among them. However, subgroup IIB (ZnO-NPs at a dose 400 mg/kg for 28 days) exhibited a statistically significant raise compared to subgroups IIA and IIIB. As regard subgroup IIIA (withdrawal dose of 100 mg/kg), there was a statistically significant reduction in mean area percentage of collagen as compared with subgroup IIA with no statistically significant difference compared to the control subgroups (Figure 8f).

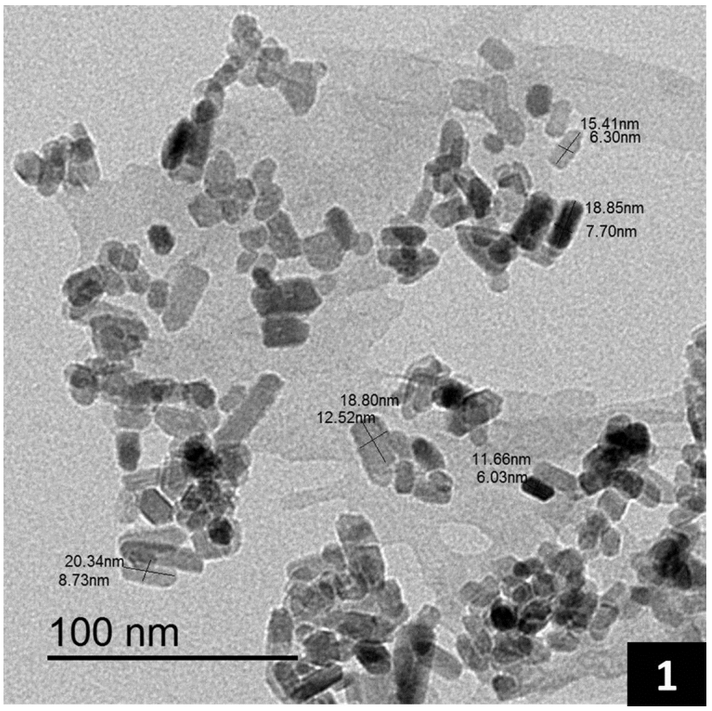

Fig. 1: An electron photomicrograph of ZnO-NPs' suspension, showing aggregates of different sizes of ZnO-NPs. Mic. Mag. X 60,000.

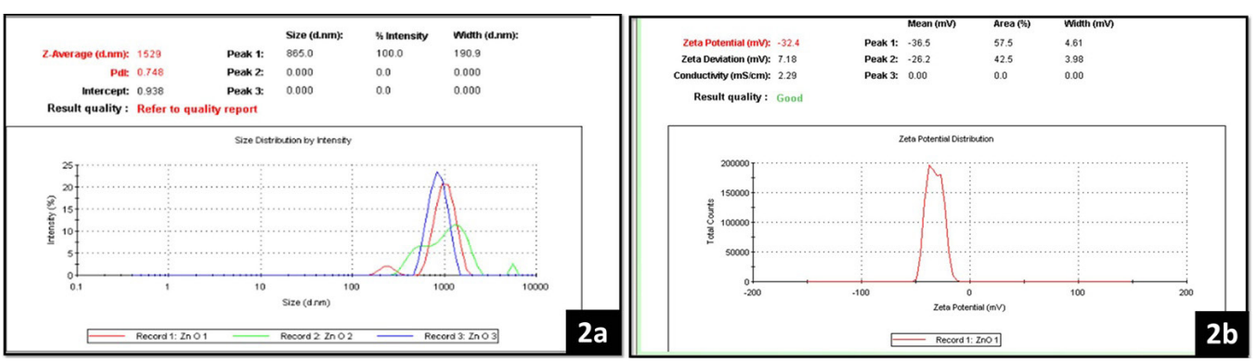

Fig. 2 (a, b): a: Hydrodynamic size distribution of ZnO-NPs, as measured by the Zetasizer. b: A zeta potential curve of ZnO-NPs.

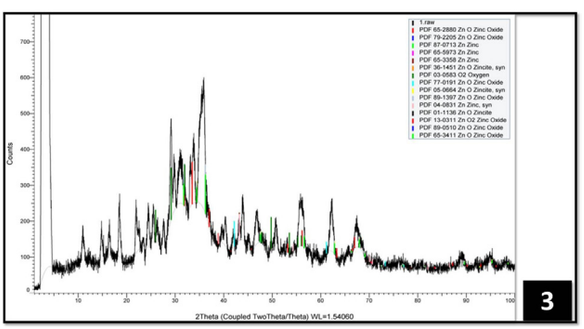

Fig. 3: XRD pattern of ZnO-NPs.

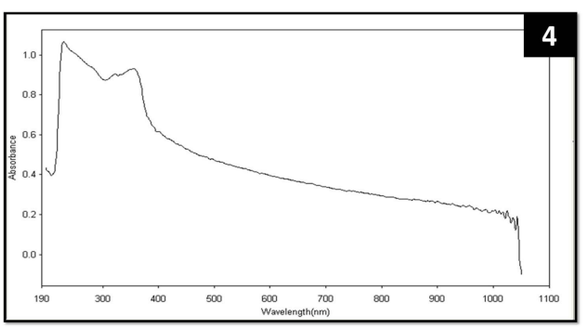

Fig. 4: UV spectrum for different sizes of ZnO-NPs.

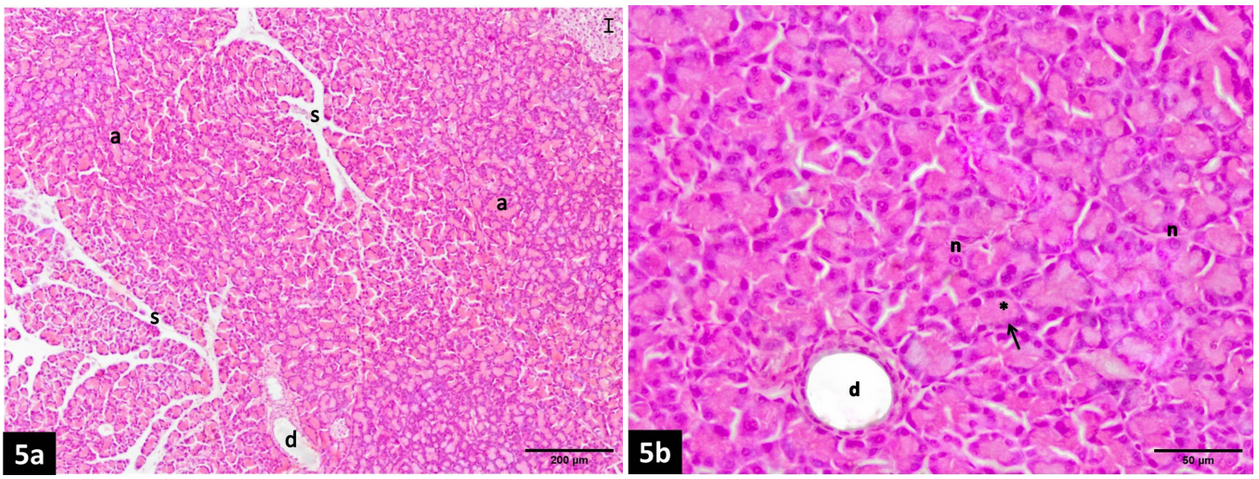

Fig. 5 (a, b): Photograph of sections of pancreas of the control subgroups (subgroups IA& IB) stained with H&E stain demonstrating: **a:** classical pancreatic lobules separated by delicate connective tissue septa (s). The secretory acini (a) are closely packed, with scattered islets of Langerhans (I) in between. **b:** pancreatic acini lined by acinar cells with apical acidophilia (asterisk) and basal basophilia (arrow). The cells have basal rounded and vesicular nuclei (n) with prominent nucleoli. d; interlobular duct. Mic. Mag. a X 100, b X 400.

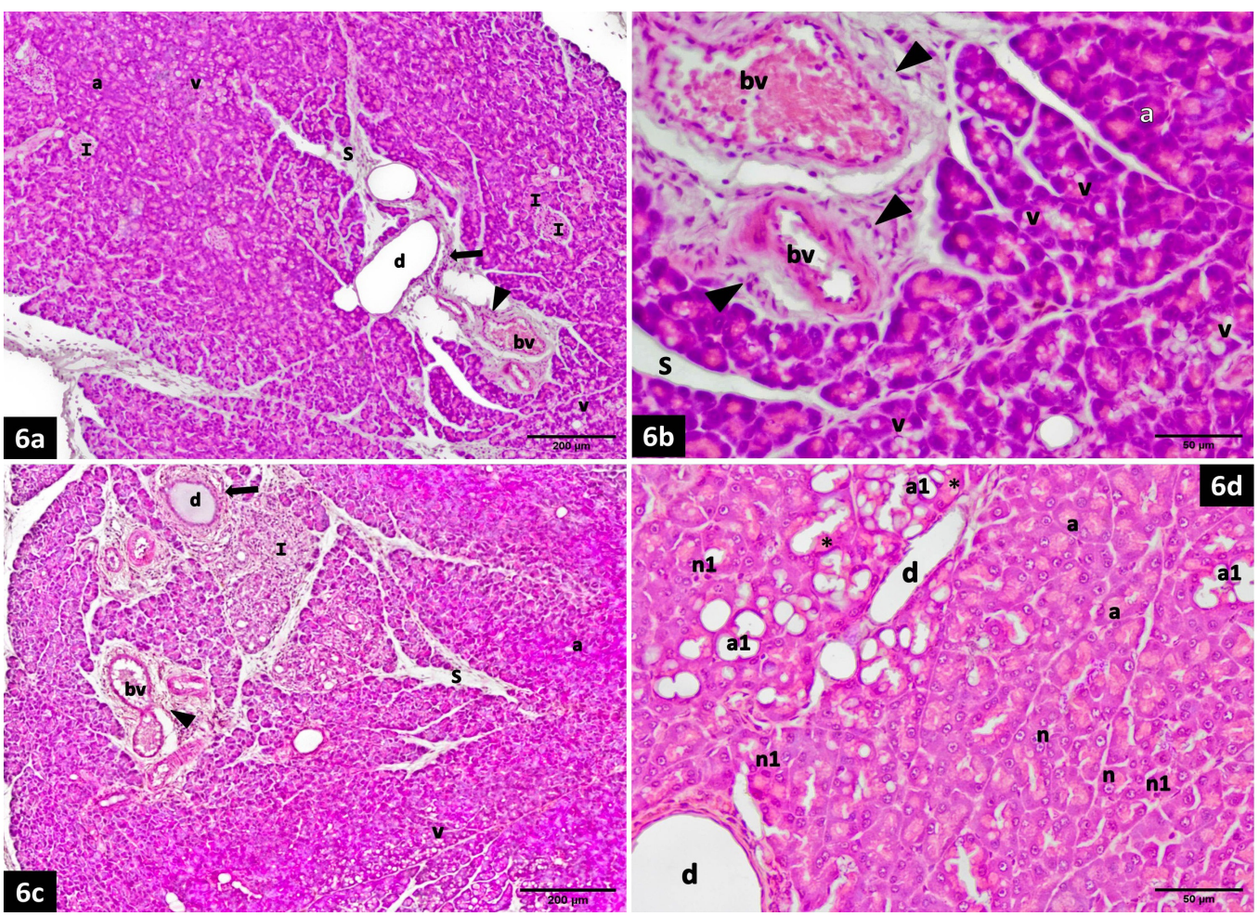

Fig. 6 (a-d): Collective photograph of sections of pancreas of the group II (ZnO-NPs treated group) stained with H&E stain. **a, b:** Subgroup IIA (received 100 mg/kg for 28 days) showing some acini lined by vacuolated acinar cells (v), while others (a) appear normal. Dilated interlobular ducts (d) with flattening of their lining cells and periductal cellular infiltration (thick arrow) in a. Dilated and congested blood vessels (bv) with perivascular cellular infiltration (arrowheads) are also seen. S; interlobular septa, I; islets of Langerhans in a. **c, d:** Subgroup IIB (received 400 mg/kg for 28 days) exhibiting some normal acini (a), while others show cytoplasmic vacuolation (v) in c with localized foci of extensively vacuolated distorted pancreatic acini (a1) in d. Interlobular septa (s) appear thickened in c. Periductal (thick arrow) and perivascular (arrowhead) inflammatory cellular infiltrate are seen in c. Some cells show hypereosinophilic cytoplasm (asterisk) in d. Some nuclei (n) appear vesicular with prominent nucleoli, while others (n1) appear dark and shrunken in d. Dilatation of interlobular ducts (d) is observed, with flattening of their lining cells. bv; blood vessel, I; islets of Langerhans in c. Mic. Mag. a&c X 100, b&d X 400.

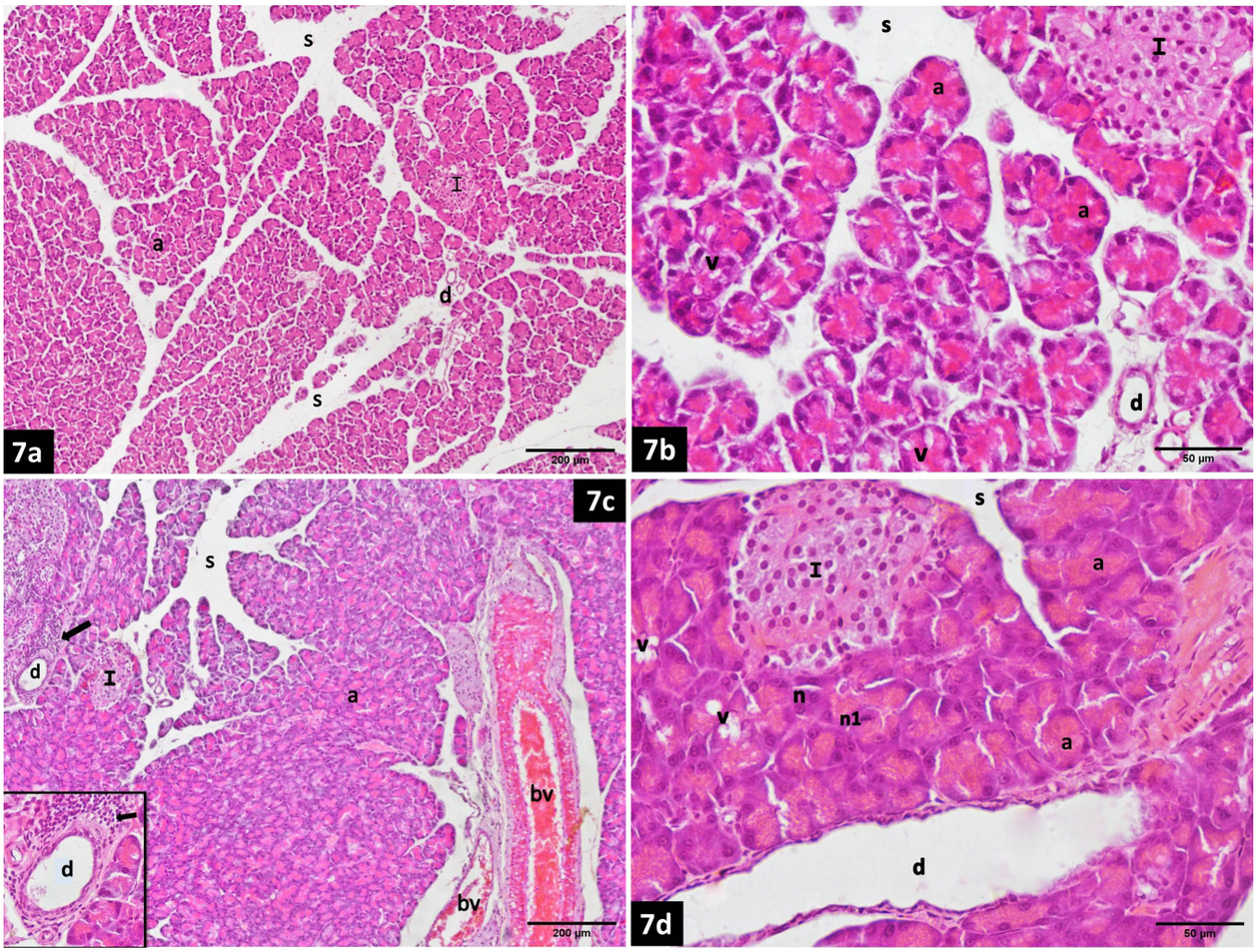

Fig. 7 (a-d): Collective photograph of sections of pancreas of the group III (withdrawal group) stained with H&E stain. **a, b:** Subgroup IIIA (withdrawal of dose 100mg/kg) illustrating widening of interlobular septa (s). The acini (a) mostly appear normal with basal basophilia and apical acidophilia. Few acinar cells appear with cytoplasmic vacuoles (v) in b. d; interlobular ducts, I; islets of Langerhans. **c, d:** Subgroup IIIB (withdrawal of dose 400 mg/kg) showing widening of the interlobular septum (s) and congestion of the blood vessels (bv) in a thickened interlobular septum in c. The acini (a) mostly appear normal but some acini show cytoplasmic vacuoles (v) in d. Marked periductal cellular infiltration (thick arrow) is seen in c and the inset. Dilatation of the interlobular duct (d), with flattening of the lining cells is noticed. Most of the nuclei (n) are vesicular, while few nuclei (n1) appear pyknotic. I; islets of Langerhans. Mic. Mag. a&c X 100, b, inset &d X 400.

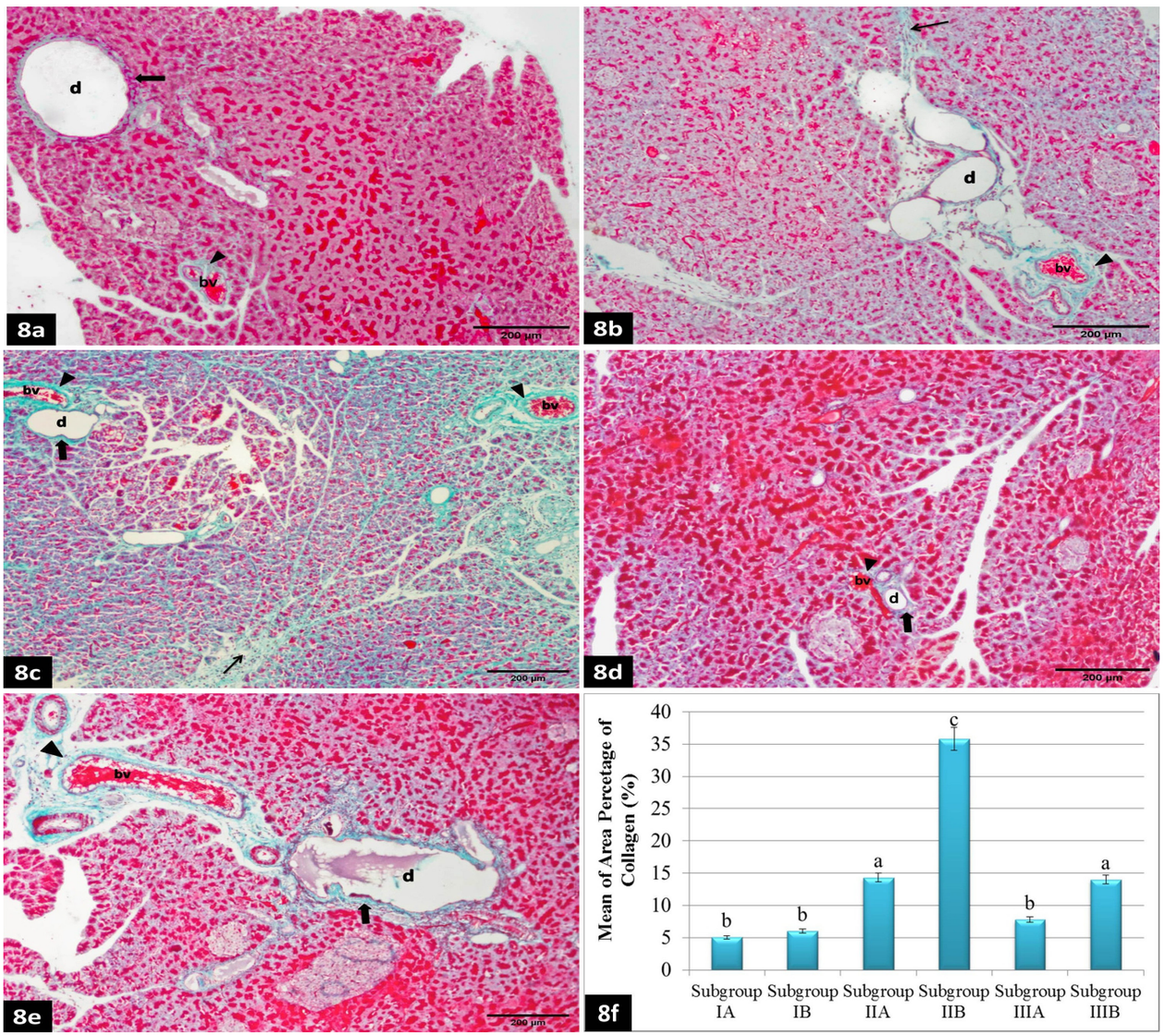

Fig. 8 (a-e): Collective photograph of Gomori's trichrome stained sections of pancreas. a: Group I (control group): Minimal amount of collagen fibers in the periductal (thick arrow), perivascular (arrowhead) areas and in the interlobular septa are seen. b: subgroup IIA (received 100 mg/kg for 28 days) increased amount of interlobular (arrow) and perivascular (arrowhead) collagen fibers are noticed. c: subgroup IIB (received 400 mg/kg for 28 days) massive collagen fibers deposition in the interlobular septa (arrow), around the ducts (thick arrow) and around the blood vessels (arrowheads) are observed. The organization of collagen fibers is greatly extended to be demonstrated between pancreatic acini. d: subgroup IIIA (withdrawal of dose 100 mg/kg) nearly normal perivascular (arrowhead) and periductal (thick arrow) collagen distribution. e: subgroup IIIB (withdrawal of dose 400 mg/kg) showing moderate amount of perivascular (arrowhead) and periductal (thick arrow) collagen fibers in thickened interlobular septa. bv; blood vessel, d; interlobular duct. Mic. Mag. a-e X 100

Fig. 8f: Histogram illustrating comparison between the evaluated subgroups based on the mean area percent of collagen. Mean with common letters are not statistically significant (i.e. Means with different letters are statistically significant).

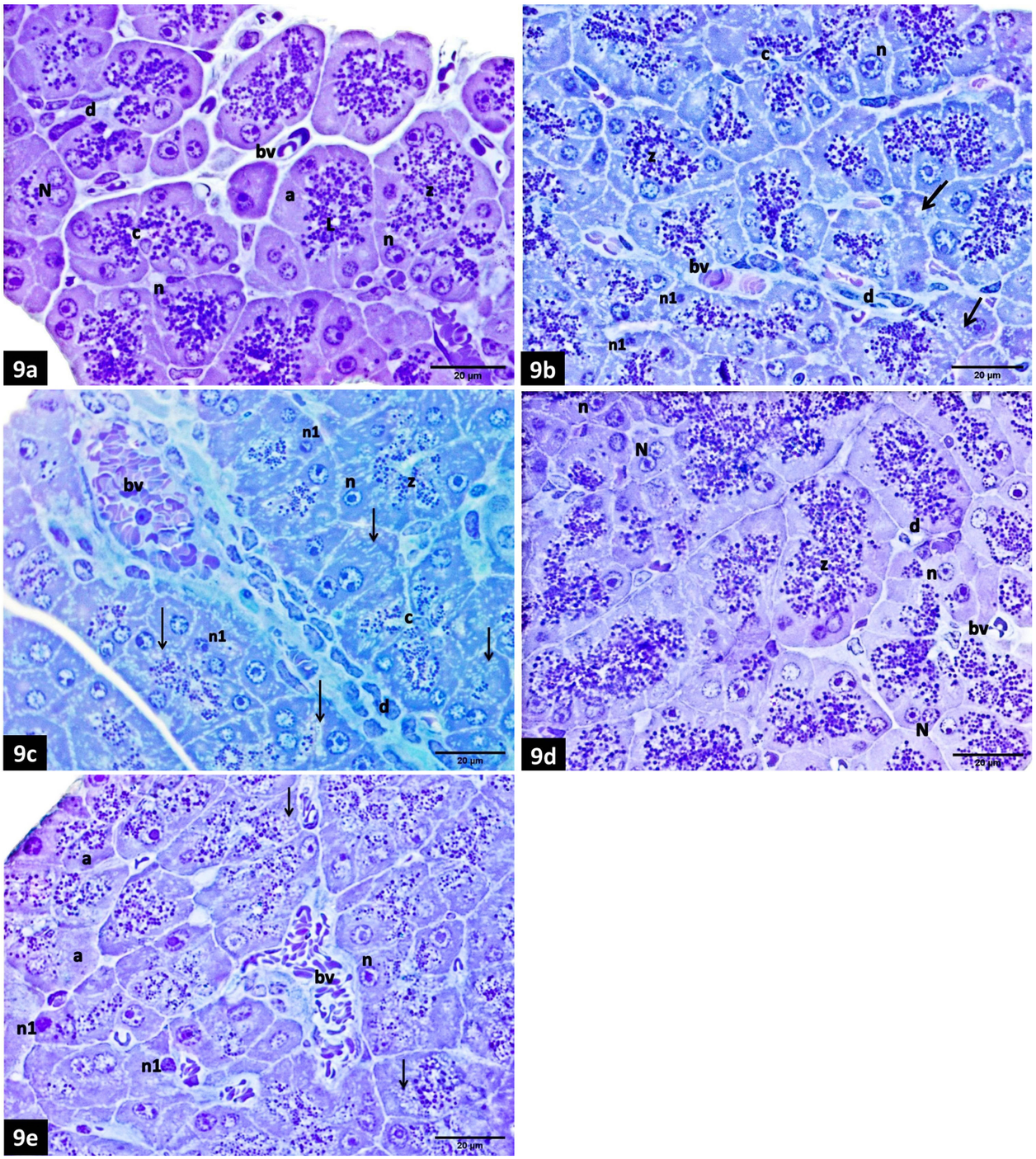

Fig. 9 (a-e): Collective photograph of toluidine blue stained semithin sections of pancreas, a: Group I (control group): normal pancreatic acini (a) with well-defined outlines. They are lined by pyramidal cells with apical zymogen granules (z). The nuclei (n) are basally located and they appear regular, rounded and vesicular with prominent nucleoli. Few acinar cells appear binucleated (N). Note the centroacinar cell (c) in the middle of the acinar lumen. An intralobular duct (d) is seen lined by cuboidal cells. L; lumen, bv; blood vessel. b: subgroup IIA (received 100 mg/kg for 28 days): acinar cells with cytoplasmic vacuolations (arrows). Most of the nuclei (n) appear vesicular with prominent nucleoli, while few nuclei (n1) appear small and deeply stained. c; centroacinar cell, z; zymogen granules, d; intralobular duct, bv; blood vessel. c: subgroup IIB (received 400 mg/kg for 28 days): acinar cells with many vacuoles (arrows) in the cytoplasm. Some nuclei (n) appear normal, while others (n1) are small with clumped chromatin. A dilated congested blood vessel (bv) is seen in the interlobular septum. c; centroacinar cell, z; zymogen granules, d; interlobular duct. d: subgroup IIIA (withdrawal of dose 100 mg/kg): showing apparently normal pattern of pancreatic acini with well-defined outlines. The nuclei (n) mostly appear regular with normal chromatin pattern. d; intralobular duct, z; zymogen granules, bv; blood vessel, N; binucleated cells. e: subgroup IIIB (withdrawal of dose 400 mg/kg): some acinar cells show cytoplasmic vacuolations (arrows), while others (a) are nearly normal. Some of the nuclei (n) appear vesicular with nearly normal chromatin pattern, while others (n1) show condensed chromatin. Mic. Mag. a-e x 1000.

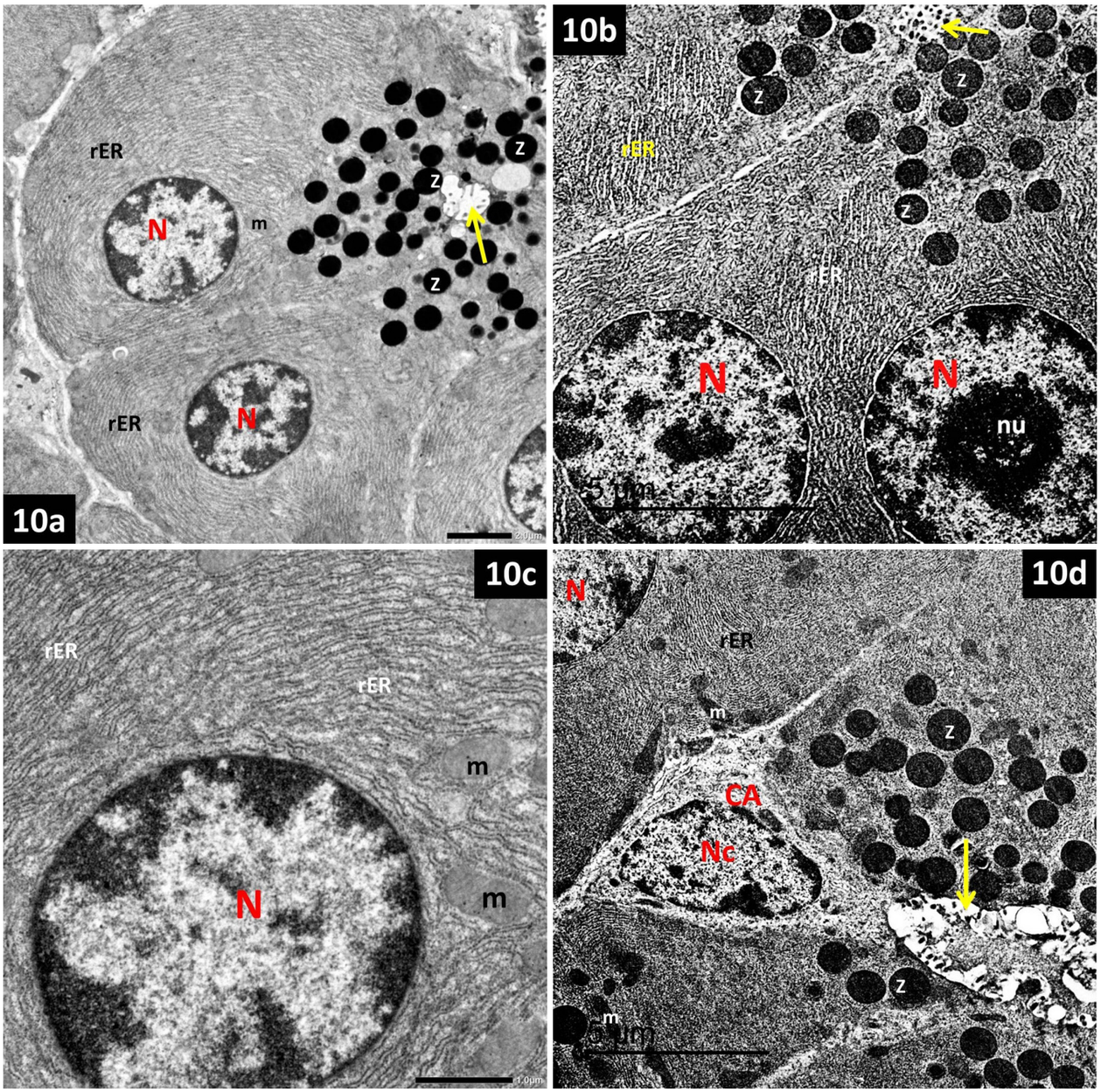

Fig. 10 (a-d): Electron micrographs of the exocrine pancreas of rats of the control subgroups (subgroups IA& IB) depicting: a: pancreatic acinus lined by pyramidal cells. The cells surround a narrow lumen (yellow arrow). Electron dense zymogen granules (Z) occupy the upper part of the cells. The nuclei (N) appear regular and euchromatic. The basal part of the cytoplasm is filled with numerous parallel cisternae of rough endoplasmic reticulum (rER). m; mitochondria. b: binucleated acinar cell. The nuclei (N) appear regular with their normal chromatin distribution and prominent nucleolus (nu). yellow arrow; lumen, Z; zymogen granules, rER; rough endoplasmic reticulum. c: part of a control pancreatic acinar cell, showing prominent rough endoplasmic reticulum (rER) with flat and parallel cisternae. The nucleus (N) is regular and euchromatic depicting its normal chromatin pattern. m; mitochondria. d: part of a control pancreatic acinus, showing many rounded electron dense zymogen granules (Z) of variable sizes occupying the apical part of the acinar cells. The cytoplasm shows well-developed rough endoplasmic reticulum (rER). Note, centroacinar cell (CA) with its cytoplasm of low electron density and few organelles. N; nucleus of acinar cell, Nc; nucleus of centroacinar cell, m; mitochondria, yellow arrow: lumen of the acinus. Mic. Mag. a X 2000, b X 4000, c X 6000, d X 3000

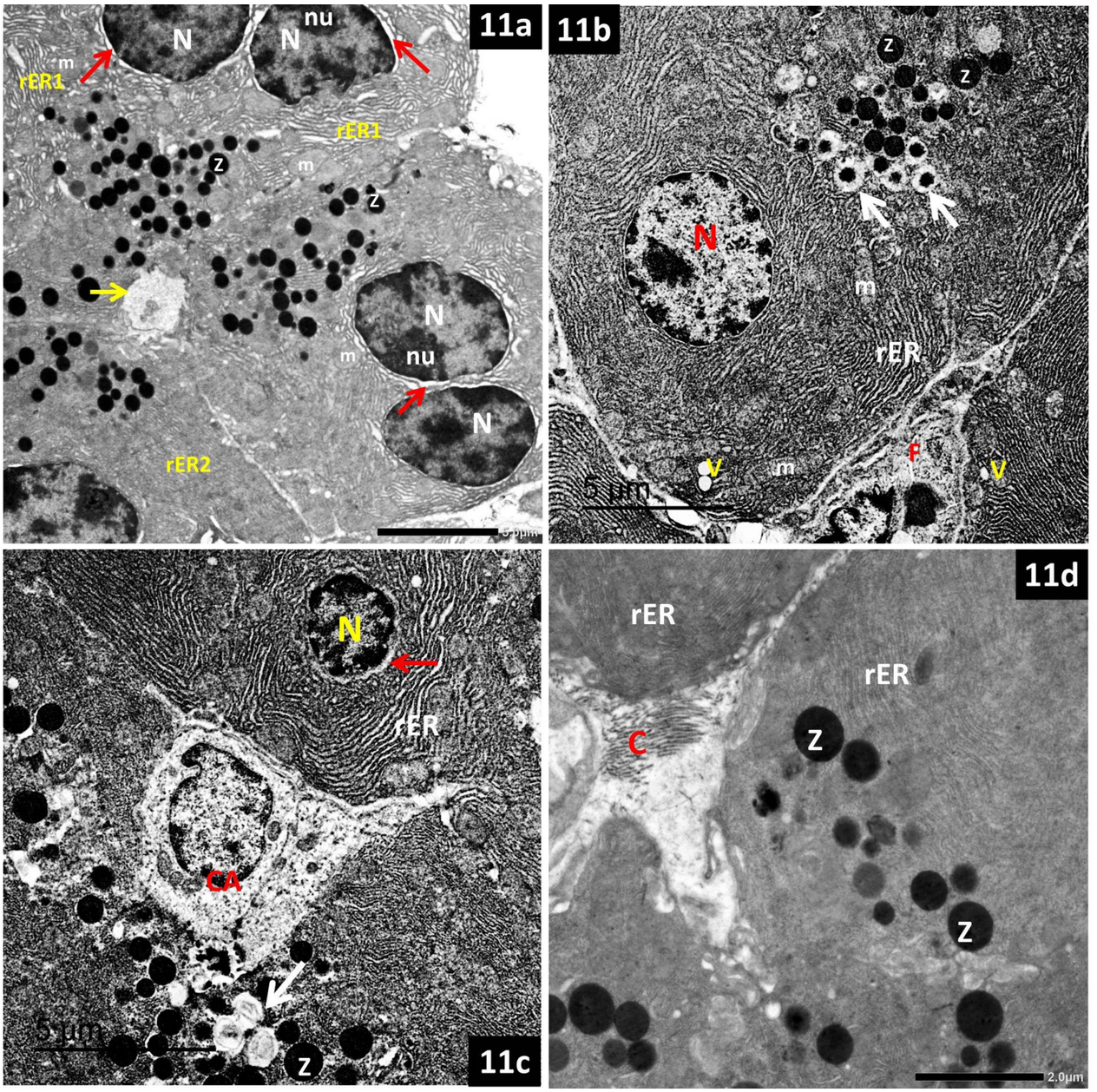

Fig. 11 (a-d): Electron micrographs of the exocrine pancreas of rats of subgroup IIA (received 100 mg/kg for 28 days) showing: a: a part of pancreatic acinus lined by binucleated pyramidal cells. The nuclei (N) are basal, euchromatic with apparent nucleoli (nu) and dilated perinuclear cisternae (red arrows). The apical cytoplasm contains zymogen granules (Z) of variable sizes and electron density. Some profiles of rough endoplasmic reticulum (rER1) appear mildly dilated, while others are normal with flat parallel cisternae (rER2). m; mitochondria, yellow arrow; lumen of the acinus. b: mild dilatation of cisternae of rough endoplasmic reticulum (rER). Some zymogen granules (Z) appear electron dense, while others have electron dense cores and electron-lucent halos (white arrows). Few vacuoles (V) are also seen in the basal cytoplasm. F; fibroblast, N; nucleus, m; mitochondria. c: parts of pancreatic acini showing nucleus (N) with irregular outline, clumped chromatin and dilated perinuclear cisterna (red arrow). Mild dilatation of cisternae of rough endoplasmic reticulum (rER) is seen. Note, zymogen granules of very low electron density (white arrow) are noticed among normal ones (Z). CA; centroacinar cell. d: collagen fibers (C) are seen in between pancreatic acinar cells. rER; rough endoplasmic reticulum, Z; zymogen granules. Mic. Mag. a X 1500, b X 2500, c X 3000, d X 4000.

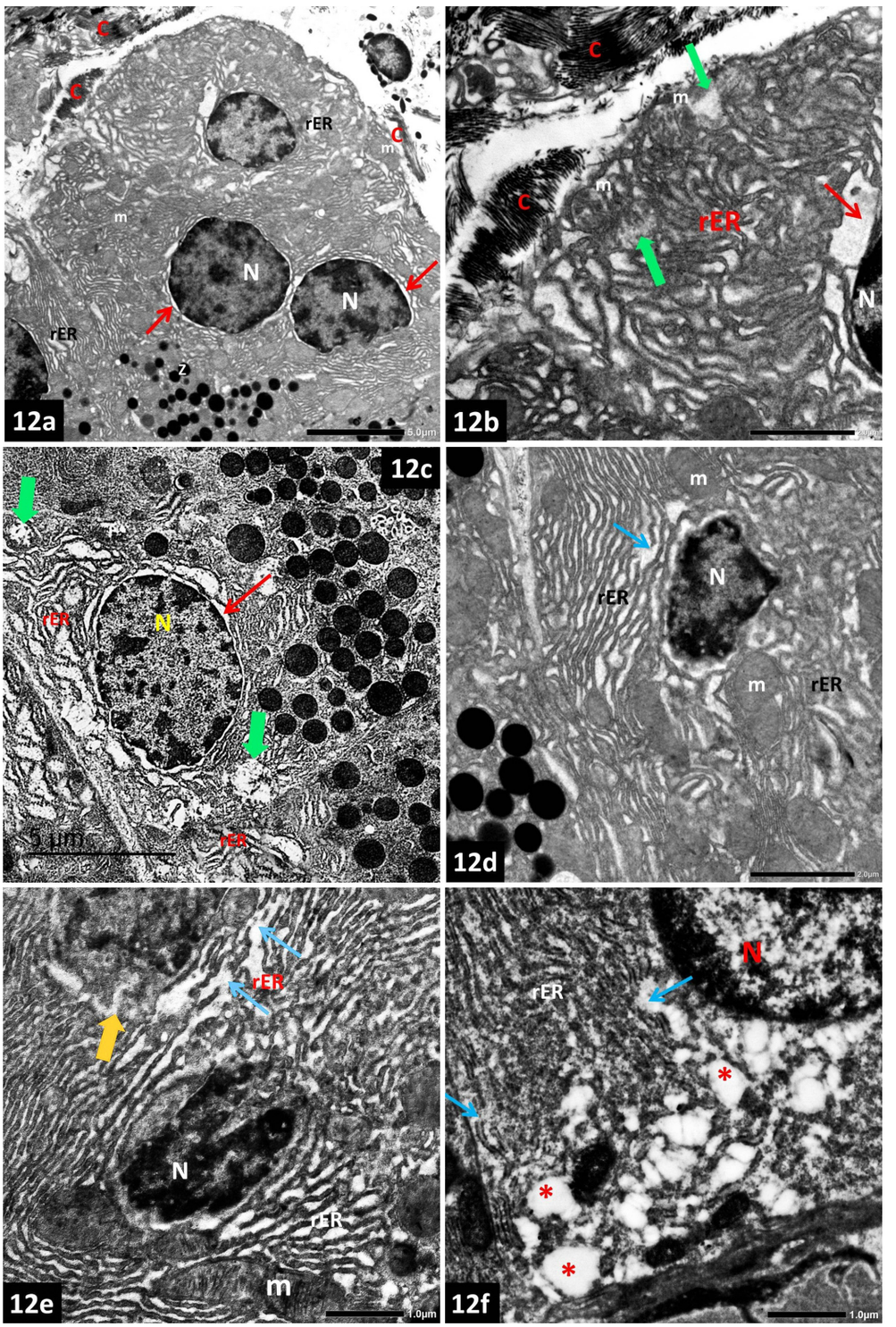

Fig. 12 (a-f): Electron micrographs of the exocrine pancreas of rats of subgroup IIB (received 400 mg/kg for 28 days) demonstrating: a: pancreatic acinar cells show euchromatic nuclei (N) with marked dilatation of perinuclear cisternae (red arrows). The cisternae of rough endoplasmic reticulum (rER) appear markedly dilated with complete loss of organization. Collage fibers (C) are seen in the inetrstitium. Z; zymogen granules, m; mitochondria. b &c: Excessive collagen fibers (C) deposition in between the cells is seen in b. The mitochondria (m) display a rise in matrix translucency and destruction of cristae (green arrows). Marked dilatation with complete loss of organization of cisternae of rough endoplasmic reticulum (rER) is also noticed. The perinuclear cisterna (red arrow) is obviously dilated. N; nucleus. d &e: dilatation and irregularity of the cisternae of rough endoplasmic reticulum (rER) with areas of loss of continuity (blue arrows). The nuclei (N) appear with irregular outline and condensed chromatin. Another nucleus (orange arrow) appears with indistinct boundaries and interrupted nuclear envelope in e. m; mitochondria. f: Loss of continuity (blue arrows) of cisternae of rough endoplasmic reticulum (rER) is seen. Areas of cytoplasmic rarefactions (*) are also noticed. N; nucleus. Mic. Mag. a X 1500, b&d X 4000, c X 3000, e&f X 6000.

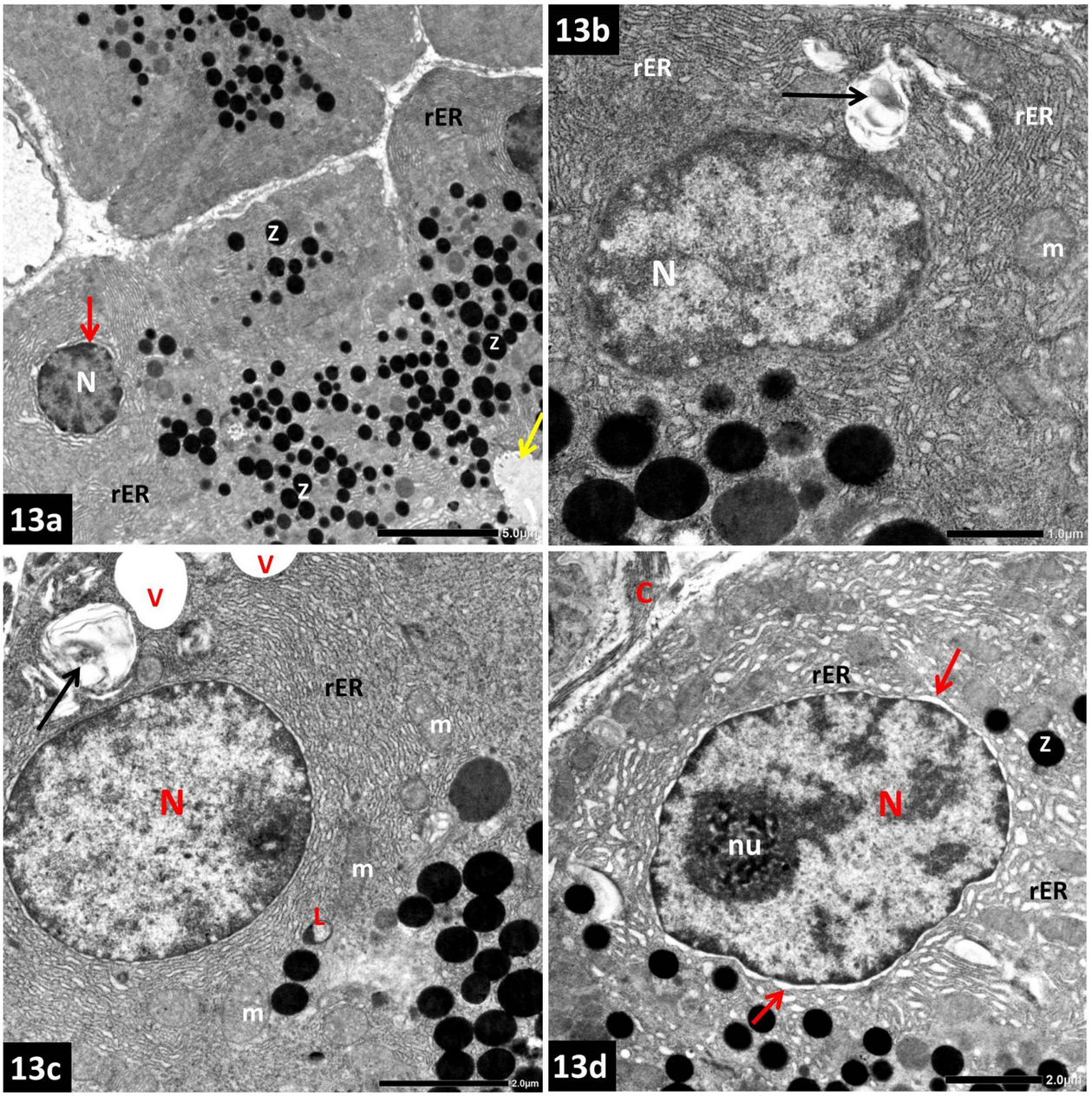

Fig. 13 (a-d): Electron micrographs of the exocrine pancreas of rats of subgroup IIIA (withdrawal of dose 100 mg/kg) exhibiting: a: pancreatic acinar cells depict apparently normal ultrastructure with electron dense zymogen granules (Z) in the apical cytoplasm towards the lumen (yellow arrow). The nucleus (N) is of regular outline and normal chromatin pattern. Mild dilatation of perinuclear cisterna is observed (red arrow). rER; rough endoplasmic reticulum. b& c: pancreatic acinar cells have euchromatic nuclei (N) and parallel well organized cisternae of rough endoplasmic reticulum (rER). Myelin figure like structures (black arrows) are also seen. Basal vacuolations are observed in c. m; mitochondria, L; lysosome. d: part of acinar cell with mild dilated cisternae of rough endoplasmic reticulum (rER). The nucleus (N) is euchromatic vesicular with apparent nucleolus (nu) and mild dilatation of perinuclear cisterna (red arrow). Collagen fibers (C) are found in between the cells. Z; zymogen granules. Mic. Mag. a X 1500, b X 6000, c X 4000, d X 3000.

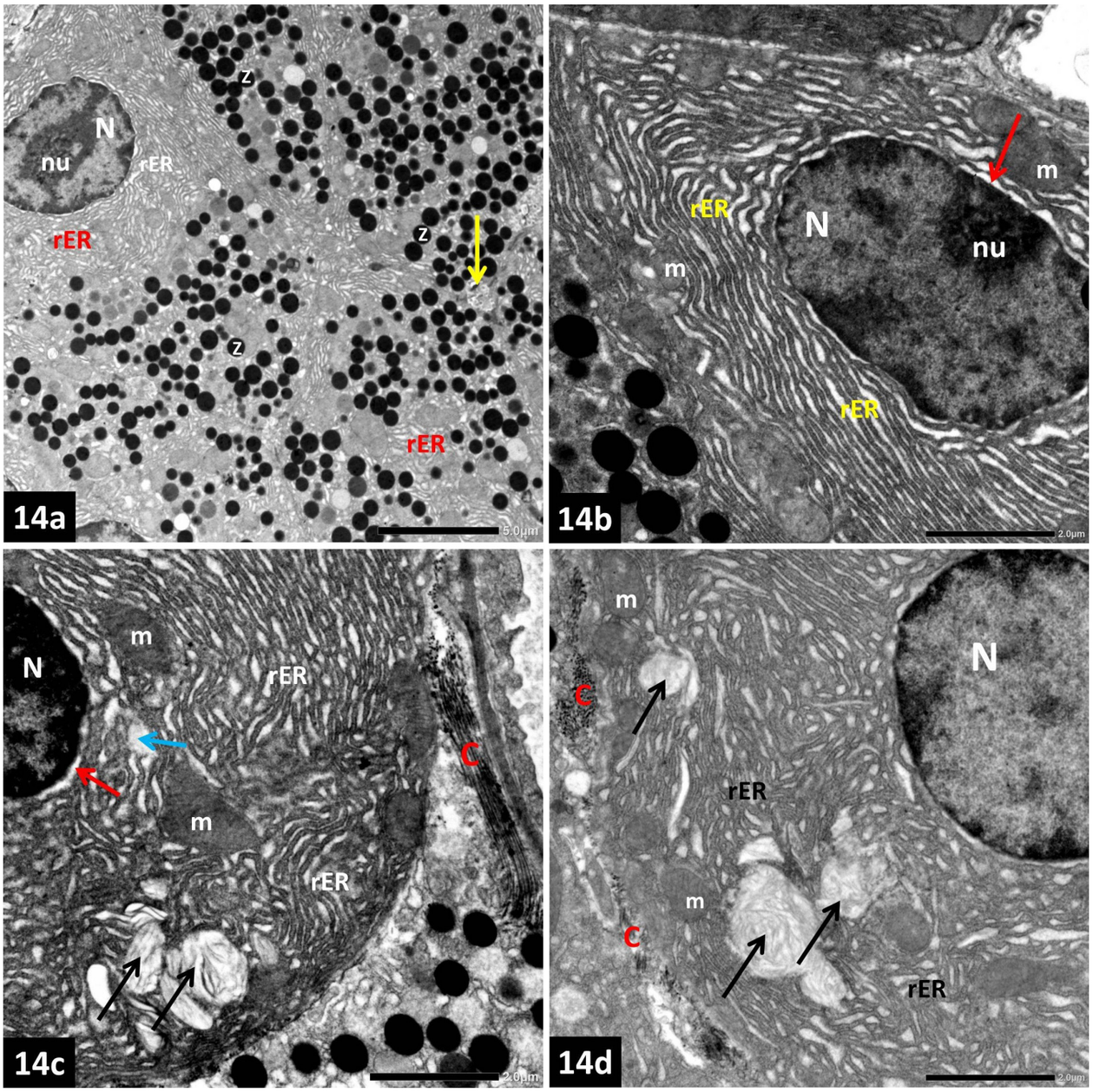

Fig. 14 (a-d): Electron micrographs of the exocrine pancreas of rats of subgroup IIIB (withdrawal of dose 400 mg/kg) a: part of pancreatic acinus lined by pyramidal cells with euchromatic nucleus (N) and prominent nucleolus (nu). Cisternae of rough endoplasmic reticulum (rER) are dilated. Z; zymogen granules, yellow arrow; lumen of acinus. b, c & d: pancreatic acinar cells have mildly dilated cisternae of rough endoplasmic reticulum (rER). Some cisternae show discontinuations (blue arrow) in c. Nuclei (N) are euchromatic in b and d while c exhibits heterochromatic nucleus (N). Myelin figure like structures (black arrows) and extracellular collagen fibers (C) are detected in c and d. Dilated perinuclear cisternae are seen in b and c. nu; nucleolus, m; mitochondria. Mic. Mag. a X 1500, b, c &d X 4000.

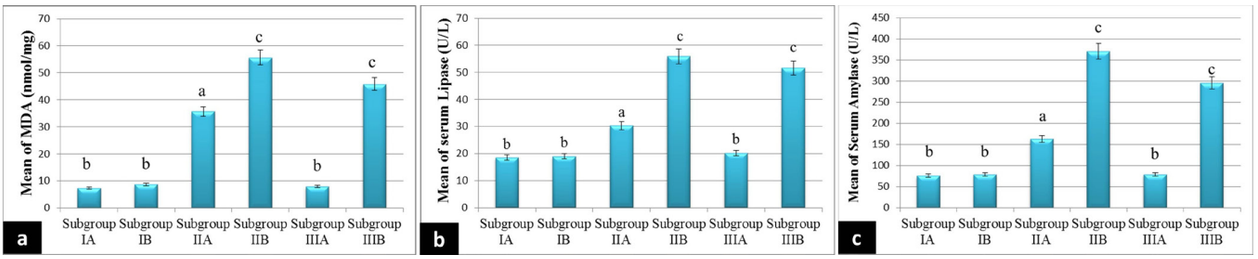

Histogram: representing the mean values of: a; Malondialdehyde (MDA), b; serum lipase, c; serum amylase among the studied subgroups. Mean with common letters are not statistically significant (i.e. Means with different letters are statistically significant).

DISCUSSION

Nanotechnology has the ability to dramatically change many aspects of our life. Owing to their large surface area and strong reactivity, nanoparticles have a significant use in many fields like biomedicine, microelectronics, and material engineering[36]. However, benefits can be accompanied by threats to the human health and environment. There have been significant concerns about the safety and public acceptability of this technology, especially in the last ten years, due to the lack of knowledge about their potential detrimental effects[37].

Among various metal oxides, ZnO-NPs are one of most commenly utilized nanostructured materials due to their versatile physical and chemical properties as well as their ease of synthesis. They are produced extensively on a global scale, being among the top five NPs now utilised in everyday consumer goods[38]. This in turn, increases the chance of their exposure, whether in the environment or in the idustry and work places. So, there is an emerging need to investigate their toxicity.

ZnO-NP-mediated cytotoxicity is probably caused by a variety of factors: the possible discharge of toxic ions from metallic NPs, the intrinsic characteristics of the NPs and finally the dose of NPs[39].

In the present study, microscopic examination of the pancreatic acinar cells of subgroups IIA and IIB rats (received ZnO-NPs doses of 100 mg/Kg and 400 mg/Kg for 28 days respectively) revealed structural changes which were more evident in subgroup IIB. Cytoplasmic vacuolations up to the distortion of some acini and hypereosinophilic cytoplasm were found. In subgroup IIB, the nuclei of some acinar cells appeared shrunken and pyknotic.

The light microscopic findings were supported ultrastructurally. On electron microscopic study, cytoplasmic vacuolations and rarefaction, dilatation, loss of organization and sometimes discontinuation of the rER cisternae together with variable changes in zymogen granules were reported. Some nuclei were irregular with peripheral chromatin condensation and dilated perinuclear cisternae. Few nuclei appeared with indistinct boundaries and interrupted nuclear envelope. Mitochondrial degeneration in the form of loss of cristae and decrease matrix density was also seen.

A key factor in the toxicity of ZnO-NPs is the dissolution of the particles in the biological environments. Senapati *et al*.[40] demonstrated that those NPs after being enodocytosed, fuse with the endosomes that afford a medium of a low pH (about 5.5), which is quite promising for dissolution of Zn2+ ions. This is followed by their leakage from the endosomes with increase of the cytosolic Zn2+ content which Singh[41] identified as the primary cause of the disruption to cellular membranes, the onset of inflammatory reactions, DNA damage, and the death of mammalian cells.

Another explanation for the toxicity of ZnO-NPs is the oxidative action of these nano-class materials[18]. Previous researches demonstrated that exposure to ZnO-NPs led to oxidative stress both in *vitro* and in *vivo*[42-44]. Generation of reactive oxygen species (ROS) can occur impulsively when ZnO-NPs are subjected to the acidic environment of lysosomes or after their interaction with the oxidative organelles, such as the mitochondria[45]. Even after only a little number of ZnO-NPs has been integrated into the cells, the cells are then unable to handle the residues. Accumulation of ROS causes organelle dysfunction, inflammatory responses, lipid peroxidation and DNA damage[18].

Moreover, Attia *et al*.[46] suggested that ROS production initiated by the NPs, hinders the production of antioxidant enzymes, such as superoxide dismutase, catalase, peroxidases, reductases and transferases. Therefore, cells try to stimulate nuclear factor kappa B (NF-kB) transcription factor which participates in these antioxidant enzymes' mRNA transcription. Unfortunately, cells are unable to reestablish the usual balance when soluble NPs are present, which causes cytotoxicity and ultimately cell death.

Furthermore, Wang *et al*.[25] demonstrated that ZnO-NPs' exposure induced a significant Ca2+ release from intracellular storage sites in response to oxidative stress which can lead to mitochondrial perturbation. Mitochondrial matrix Ca2+ overload favors opening of the mitochondrial permeability transition (MPT) pores, enhancing generation of ROS and triggering cytochrome C release which initiates the apoptotic degradation. Such an interpretation is consistent with our histology observations in the form of hypereosinophilic cytoplasm and dark

shrunken nuclei with condensation of their chromatin in subgroup IIB.

In our study, the nuclear changes observed in the treated group may have contributed to oxidative stress which leads to DNA damage, as ROS could interact with thymine of the nuclear DNA producing single stranded breaks[47]. Also, it was proved that metal NPs can diffuse through the nuclear pore complexes or have access to the genes when the nuclear membrane dissolves during mitosis inducing direct physical harm to the nuclear genetic material through interactions with DNA or DNA-related proteins[48].

The observed cytoplasmic vacuolations in the current work could be attributed to disturbed cell membrane function by hydrogen peroxide (H_2O_2) which is one of the peroxides produced during oxidative stress. H_2O_2 alters the hydrophobic interactions between adjacent chains of cell membrane phospholipids resulting in serious biologic consequences as cellular hydropic degeneration[49].

In addition, the cytoplasmic rarefaction seen in electron microscopic examination in some pancreatic acinar cells of subgroup IIB may be explained by the failure of energy-dependent Na+-K+ ion pumps in the plasma membranes owing to lipid peroxidation, which causes intracellular Na+ accumulation and gradual osmolarity changes, which eventually allow water to enter the cells. As cell increases in volume, the cytoplasm is diluted without an associated increase in cytoplasmic organelles, thus, electron-lucent areas of cytoplasmic matrix appear separating the organelles and the inclusions[50,51].

Dilated perinuclear and rER cisternae observed in group II (ZnO-NPs treated group) was an evident ultrastructural finding that could indicate increased secretory function. Previous studies attributed this cisternal dilatation to protein synthetic stages with granule secretion[52,53]. The decrease in number and electron density of some zymogen granules together with swollen endoplasmic reticulum was also proved in acute pancreatitis induced by caerulein and lipopolyasccharide[54]. This hypothesis was supported by the highly elevated serum levels of amylase and lipase in rats treated with ZnO-NPs compared to the control group. It has been demonstrated that a high serum amylase or lipase level can be used to diagnose pancreatitis[55]. In addition, Ghadially[56] attributed this dilation to the ingress of water into the cellular membranes.

One of the most important sensitive cell organelles that all NPs have the potential to adversely influence is the mitochondria[57]. Mitochondrial alterations seen in acinar cells of subgroup IIB were in agreement with Han *et al*.[58] who suggested that ROS production may mediate these changes, which cause the mitochondrial cation pump to be compromised, ATP production to be reduced, and mitochondrial metabolism to be impaired. In the current study, a dose-dependently higher pancreatic MDA level was found in rats exposed to ZnO-NPs, which is more pronounced in subgroup IIB, indicating increased lipid peroxidation caused by oxidative stress and excessive ROS generation. The findings were compatible with the results of Khayal *et al*.[59] and Qin[60] who demonstrated lipid peroxidation as a molecular mechanism underlying ZnO-NPs-induced cell toxicity and injury.

Beside their effect on the pancreatic acini, this study proved that ZnO-NPs induced changes in other parts of the exocrine portion of the pancreas of group II. Widening in the interlobular septa could be explained by the occurrence of extravasation of fluid in the interstitial spaces; as ROS cause damage of endothelial cells membranes of the capillaries, resulting in increased microvascular permeability and extravasation of fluid[61]. As for the ducts, it was suggested that this change could be an adaptive mechanism attempted by the ductal epithelium that increases the ability of the pancreas to excrete the cytotoxic materials[62,63].

The evident interlobular, periductal and perivascular cellular infiltration in the pancreas of group II could be attributed as well to the consequence of oxidative stress induced by ZnO-NPs[24,44]. The increased oxygen free radicals cause up-regulation of genes that encode cytokines, chemokines and other inflammatory mediators such as: IL-1, IL-6, IL-8 and tumor necrosis factor-α (TNF-α)[64]. These molecules, in turn, lead to activation and invasion of polymorphonuclear leukocytes (PMNLs) that produce more ROS. Additionally, they help PMNLs to be attracted and localised to the area of inflammation. The influx of inflammatory leukocytes amplifies the pancreatic injury by stimulating trypsinogen activation within the acinar cells leading to enhanced autodigestion injury[65]. Another study similarly demonstrated that the 14-day oral administration of 20 nm ZnO-NPs to mice caused substantial damage to the stomach mucosa with infiltrating inflammatory cells in the liver and pancreas[66].

Excess collagen fibers in the exocrine pancreas of the treated group was explained by Jancsó *et al*.[67] who postulated that the loss of architectural integrity exposes fibroblasts to mechanical stress, which together with transforming growth factor B (TGF-β) and cytokines cause fibroblast to proliferate and migrate to the injured region.

These findings were also supported by light microscopic examination of Gomori's trichrome stained sections of group II which revealed collagen fibers deposition in the interlobular, perivascular and periductal areas which was more evident in subgroup IIB as proved by morphometric study. Once more, this could be a sign of the highly harmful impact of ROS which stimulate collagen synthesis that in turn promoted fibrosis[68]. Peng *et al*.[69] and Genah *et al*.[70] hypothesized that increase production of cytokines and chemokines results in increased fibroblast activation, with subsequent increased collagen synthesis.

On the other hand, such increased collagen distribution was explained by Spanehl *et al*.[71] who attributed it to the presence of stellate cells. Both the rat and human pancreas have been revealed to contain pancreatic stellate cells (PSCs), which have been linked to the emergence of pancreatic fibrosis. Normally, they involve about 4-7%

of the total cell mass in the gland[72]. The inactive PSCs are triangular, lipid containing cells mainly seen in the perivascular and periductal areas. When triggered, they lose their lipid droplets develop a fibroblast-like morphology, proliferate and upregulate myofibroblast markers such as: smooth muscle actin[73]. They develop the ability to synthesise collagen types I, II and fibronectin, and migrate to periacinar regions[74].

The microscopic and biochemical evidences provided in the current work demonstrated that ZnO-NPs induce toxicity to the pancreatic acini especially with higher doses. The study was further extended to investigate whether a one month withdrawal period is sufficient to improve or eliminate these histological changes. Unfortunately, ZnO-NPs withdrawal didn't repair the pancreatic damage completely at high doses despite of improvement at lower ones.

Chronic inorganic nanoparticle exposure has been linked to fibrosis, inflammation, and hindered clearance[75,76]. This explained the persistent changes detected in subgroup IIIB.

However, a striking ultrastructure finding in the withdrawal group was the presence of myelin figures like structures which were most probable a whorled pattern of dilated rER. This was explained by some investigators[77,78] as a form of ER stress and unfolded protein response in which ER transmembrane receptors notice the onset of ER stress and start the unfolded-protein response (UPR) to reestablish normal ER function. This was accompanied by decrease exocytosis which was evident in our biochemical results by significant reduction of serum amylase and lipase in withdrawal subgroups in comparison with ZnO- NPs treated subgroups. It was found that ZnO-NPs exposure triggers ER stress responses both in *vivo* and in *vitro*[79]. Hepatotoxicity in mice has been associated with ZnO-NP-mediated ER stress and apoptosis[80].

However, any improvement in the structural or biochemical changes of the pancreas in group III might indicate the occurrence of a regenerative process in addition to the ongoing degenerative one. It was proposed that different cell types became involved in the process of repair and regeneration relatively immediately after the point of injury. These cells include not only the pancreatic acinar cells, but also the ductal epithelial cells, inflammatory cells of the immune system, resident fibroblasts and the pancreatic stellate cells[81].

In pancreatitis models, two distinct forms of regeneration have been postulated to take place. In the conventional regeneration mechanism, new acinar cells are not generated from newly differentiated cells from an external source, such as stem cells, but rather from proliferation of the remaining surviving cells[82]. In the second regeneration mode, the degranulated acinar cells are thought to undergo redifferentiation, returning to a healthy and functional acinar state[83].

The intimate cell-to-cell communication is a third important component of exocrine regeneration. For instance, the severity of pancreatitis is exacerbated and necrosis persists in Connexin-32 transgenic mice when gap junctional communication between acinar cells is impaired[84]. Another crucial factor in the renewal of acinar cells is the ductal system's vitality[85].

CONCLUSION

The present study came to the conclusion that oral administration of ZnO-NPs is coupled with a variety of microscopic alterations in pancreatic acini that are dose-dependent. The pancreatic and the oxidative stress markers both significantly increased in conjunction with the microscopic alterations. These changes were reversible at low doses but partially improved with high doses. It was recommended that other further studies should be conducted to look for the protective medicine, especially with higher doses.

CONFLICT OF INTERESTS

There are no conflicts of interest.

REFERENCES

1. Chausali N, Saxena J, Prasad R. Recent trends in nanotechnology applications of bio-based packaging. Journal of Agriculture and Food Research 2022; 7:100257. https://doi.org/10.1016/j.jafr.2021.100257.
2. Nikzamir M, Akbarzadeh A, Panahi Y. An overview on nanoparticles used in biomedicine and their cytotoxicity. Journal of Drug Delivery Science and Technology 2021 ; 61:102316. https://doi.org/10.1016/j.jddst.2020.102316.
3. Farzaneh M, Mokhtari S, Moraveji SF, Sayahpour FA, Masoudi NS, Javadi A, *et al*. In *vitro* investigation of zinc oxide nanoparticle toxic effects in spermatogonial cells at the molecular level. Chemico-Biological Interactions 2022; 351:109687. https://doi.org/10.1016/j.cbi.2021.109687.
4. Nasrollahzadeh M, Sajadi SM, Sajjadi M, Issaabadi Z. An introduction to nanotechnology. In Interface science and technology 2019;28:1-27. Elsevier. https://doi.org/10.1016/B978-0-12-813586-0.00001-8.
5. Taran M, Safaei M, Karimi N, Almasi A. Benefits and application of nanotechnology in environmental science: an overview. Biointerface Research in Applied Chemistry 2021;11(1):7860-70. https://doi.org/10.33263/BRIAC111.78607870.
6. Bayda S, Adeel M, Tuccinardi T, Cordani M, Rizzolio F. The history of nanoscience and nanotechnology: from chemical–physical applications to nanomedicine. Molecules 2019; 25(1):112. https://doi.org/10.3390/molecules25010112.
7. Svendsen C, Walker LA, Matzke M, Lahive E, Harrison S, Crossley A, *et al*. Key principles and operational practices for improved nanotechnology environmental exposure assessment. Nat Nanotechnol 2020; 15(9):731-42. http://dx.doi.org/10.1038/s41565-020-0742-1.

8. Saleem S, Jameel MH, Rehman A, Tahir MB, Irshad MI, Jiang ZY, *et al*. Evaluation of Structural, Morphological, Optical, and Electrical Properties of Zinc Oxide Semiconductor Nanoparticles with Microwave Plasma Treatment for electronic device Applications. Journal of Materials Research and Technology 2022, 19: 2126-2134. https://doi.org/10.1016/j.jmrt.2022.05.190.

9. Singh TA, Sharma A, Tejwan N, Ghosh N, Das J, Sil PC. A state of the art review on the synthesis, antibacterial, antioxidant, antidiabetic and tissue regeneration activities of zinc oxide nanoparticles. Advances in Colloid and Interface Science 2021;295:102495. https://doi.org/10.1016/j.cis.2021.102495.

10. Singh TA, Das J, Sil PC. Zinc oxide nanoparticles: A comprehensive review on its synthesis, anticancer and drug delivery applications as well as health risks. Advances in Colloid and Interface Science 2020; 286:102317. https://doi.org/10.1016/j.cis.2020.102317.

11. Patrón-Romero L, Luque PA, Soto-Robles CA, Nava O, Vilchis-Nestor AR, Barajas-Carrillo VW, *et al*. Synthesis, characterization and cytotoxicity of zinc oxide nanoparticles by green synthesis method. Journal of Drug Delivery Science and Technology 2020; 60:101925. https://doi.org/10.1016/j.jddst.2020.101925.

12. Asha S, Bessy TC, Sherin JJ, Kumar CV, Bindhu MR, Sureshkumar S, *et al*. Efficient photocatalytic degradation of industrial contaminants by Piper longum mediated ZnO nanoparticles. Environmental Research 2022; 208:112686. https://doi.org/10.1016/j.envres.2022.112686.

13. Thummala H, Raju NV, Manasa B, Paritala V, Srikanth K, Nutalapati V. Sublethal effects of zinc oxide nanoparticles induced toxicity and oxidative stress in Pila virens: A validation of homology modelling and docking. Materials Science and Engineering: B 2022; 283:115842. https://doi.org/10.1016/j.mseb.2022.115842.

14. Jiménez-Chávez A, Solorio-Rodríguez A, Escamilla-Rivera V, Leseman D, Morales-Rubio R, Uribe-Ramírez M, *et al*. Inflammatory response in human alveolar epithelial cells after TiO2 NPs or ZnO NPs exposure: Inhibition of surfactant protein A expression as an indicator for loss of lung function. Environmental Toxicology and Pharmacology 2021; 86:103654. https://doi.org/10.1016/j.etap.2021.103654.

15. Yousef MI, Mutar TF, Kamel MA. Hepato-renal toxicity of oral sub-chronic exposure to aluminum oxide and/or zinc oxide nanoparticles in rats. Toxicology reports 2019; 6:336-46. https://doi.org/10.1016/j.toxrep.2019.04.003.

16. Liang C, Fang J, Hu J, Geng X, Liu H, Feng Y, *et al*. Toxicokinetics of zinc oxide nanoparticles and food grade bulk-sized zinc oxide in rats after oral dosages. NanoImpact 2022; 25:100368. https://doi.org/10.1016/j.impact.2021.100368.

17. Shaban E, Salaheldin K, El-Aziz A, Essam M, M Desouky H, F Elbakry H. Evaluation of acute oral toxicity of zinc oxide nanoparticles in rats. Egyptian Journal of Chemistry 2021; 64(8):1-2. https://dx.doi.org/10.21608/ejchem.2021.80810.4003.

18. Singh R, Cheng S, Singh S. Oxidative stress-mediated genotoxic effect of zinc oxide nanoparticles on Deinococcus radiodurans. 3 Biotech 2020;10(2):1-3. https://doi.org/10.1007%2Fs13205-020-2054-4.

19. Chandrasekaran S, Anusuya S, Anbazhagan V. Anticancer, anti-diabetic, antimicrobial activity of zinc oxide nanoparticles: A comparative analysis. Journal of Molecular Structure 2022; 1263:133139. https://doi.org/10.1016/j.molstruc.2022.133139.

20. Afify M, Samy N, Hafez NA, Alazzouni AS, Mahdy ES, El Mezayen HA, *et al*. Evaluation of zinc-oxide nanoparticles effect on treatment of diabetes in streptozotocin-induced diabetic rats. Egyptian Journal of Chemistry 2019; 62(10):1771-83. https://doi.org/10.21608/ejchem.2019.11350.1735.

21. Siddiqui SA, Or Rashid M, Uddin M, Robel FN, Hossain MS, Haque M, *et al*. Biological efficacy of zinc oxide nanoparticles against diabetes: a preliminary study conducted in mice. Bioscience reports 2020; 40(4). https://doi.org/10.1042/BSR20193972.

22. San Tang K. The current and future perspectives of zinc oxide nanoparticles in the treatment of diabetes mellitus. Life sciences 2019; 239:117011. https://doi.org/10.1016/j.lfs.2019.117011.

23. Vimercati L, Cavone D, Caputi A, De Maria L, Tria M, Prato E, *et al*. Nanoparticles: An experimental study of zinc nanoparticles toxicity on marine crustaceans. General overview on the health implications in humans. Frontiers in Public Health 2020; 8:192. https://doi.org/10.3389/fpubh.2020.00192.

24. Sewelam AS, Shehata MA. Nano-Zinc Oxide Induced Pancreatic Toxicity and the Ameliorating Role of Naringenin: Histological and Immunohistochemical Study. Egyptian Journal of Histology 2021; 44(4):1081-97. https://dx.doi.org/10.21608/ejh.2021.55443.1405.

25. Wang C, Lu J, Zhou L, Li J, Xu J, Li W, *et al*. Effects of long-term exposure to zinc oxide nanoparticles on development, zinc metabolism and biodistribution of minerals (Zn, Fe, Cu, Mn) in mice. PloS one 2016; 11(10):e0164434. https://doi.org/10.1371/journal.pone.0164434.

26. Alsuwayyid AA, Alslimah AS, Perveen K, Bukhari NA, Al-Humaid LA. Effect of zinc oxide nanoparticles on Triticum aestivum L. and bioaccumulation assessment using ICP-MS and SEM analysis. Journal of King Saud University-Science 2022; 34(4):101944. https://doi.org/10.1016/j.jksus.2022.101944.

27. Shuaibu AD, Rubab R, Khan S, Ali S, Shaikh AJ, Khan SA, *et al*. Comparative effects of zinc oxide nanoparticles over the interfacial properties of low concentrations of ionic surfactants at interfaces. Colloids and Surfaces A: Physicochemical and Engineering Aspects 2022; 637:128241. https://doi.org/10.1016/j.colsurfa.2021.128241.

28. Zoheir M, Medwar A, Solaiman A, Elbanawany N. Histological Study of the Effect of Zinc Oxide Nanoparticles on the Cardiomyocytes of Adult Male Albino Rats with Reference to the Role of Mitochondria. Egyptian Journal of Histology 2019; 42(3):567-82. https://dx.doi.org/10.21608/ejh.2019.7112.1065.

29. Park EJ, Jeong U, Yoon C, Kim Y. Comparison of distribution and toxicity of different types of zinc-based nanoparticles. Environ Toxicol Pharmacol 2017; 32(4):1363-74. https://doi.org/10.1002/tox.22330.

30. El-Akabawy G, El-Kholy W. Neuroprotective effect of ginger in the brain of streptozotocin-induced diabetic rats. Annals of Anatomy-Anatomischer Anzeiger 2014; 196(2-3):119-28. https://doi.org/10.1016/j.aanat.2014.01.003.

31. Fusco R, Cordaro M, Siracusa R, D'Amico R, Genovese T, Gugliandolo E, *et al*. Biochemical evaluation of the antioxidant effects of hydroxytyrosol on pancreatitis-associated gut injury. Antioxidants 2020; 9(9):781. https://doi.org/10.3390/antiox9090781.

32. Gao Y, Hou L, Wang Y, Zhang Y, Zhang S, Li Y, *et al*. Comparison of Pancreatic Damage in Rats for Two Methods of Paraquat Administration. Frontiers in Pharmacology 2021; 12:611433. https://doi.org/10.3389/fphar.2021.611433.

33. Bancroft JD, Layton C. The hematoxylins and eosin. In: Suvarna KS, Layton C, Bancroft JD (eds). Bancroft's Theory and Practice of Histological Techniques. 7th ed. New York: Churchill Livingstone; 2013: 173-85. ISBN: 978-0-7020-6864-5.

34. Hayat M A. Principles and techniques of electron microscopy: biological applications. 4th ed. Edinburgh, UK: Cambridge University Press; 2000; 37-59. ISBN: 9780713128307.

35. Suvarna KS, Layton C, Bancroft JD, editors. Bancroft's theory and practice of histological techniques E-Book. Elsevier health sciences; 2018. ISBN: 978-0-7020-6864-5.

36. Li D, Liu Y, Wu N. Application progress of nanotechnology in regenerative medicine of diabetes mellitus. Diabetes Research and Clinical Practice 2022:109966. https://doi.org/10.1016/j.diabres.2022.109966.

37. Saravanan A, Jeevanantham S, Jayasree R, Hemavathy RV, Kumar PS, Yaashikaa PR. Environmental and health effects of nanomaterials. InNanomaterials 2021: 701-711. Academic Press. https://doi.org/10.1016/B978-0-12-822401-4.00011-8.

38. Al Jabri H, Saleem MH, Rizwan M, Hussain I, Usman K, Alsafran M. Zinc Oxide Nanoparticles and Their Biosynthesis: Overview. Life 2022 ;12(4):594. https://doi.org/10.3390/life12040594.

39. Pinho AR, Martins F, Costa ME, Senos AM, da Cruz e Silva OA, Pereira MD, *et al*. In *vitro* cytotoxicity effects of zinc oxide nanoparticles on spermatogonia cells. Cells 2020; 9(5):1081. https://doi.org/10.3390/cells9051081.

40. Senapati VA, Kumar A. ZnO nanoparticles dissolution, penetration and toxicity in human epidermal cells. Influence of pH. Environmental Chemistry Letters 2018;16(3):1129-35. DOI:10.1007/s10311-018-0736-5.

41. Singh S. Zinc oxide nanoparticles impacts: Cytotoxicity, genotoxicity, developmental toxicity, and neurotoxicity. Toxicology mechanisms and methods 2019; 29(4):300-11. https://doi.org/10.1080/15376516.2018.1553221.

42. Saddick S, Afifi M, Abu Zinadaa OA. Effect of zinc nanoparticles on oxidative stress-related genes and antioxidant enzymes activity in the brain of oreochromis niloticus and tilapia zillii. Saudi J Biol Sci 2017;24(7): 1672-1678. https://doi.org/10.1016/j.sjbs.2015.10.021.

43. Jo E, Seo G, Kwon JT, Lee M, Lee B, Eom I, Kim P, Choi K. Exposure to zinc oxide nanoparticles affects reproductive development and biodistribution in offspring rats. J. Toxicol. Sci 2013;38:525–530. https://doi.org/10.2131/jts.38.525.

44. Hosseini SM, Amani R, Moshrefi AH, Razavimehr SV, Aghajanikhah MH, Sokouti Z. Chronic zinc oxide nanoparticles exposure produces hepatic and pancreatic impairment in female rats. Iranian Journal of Toxicology 2020;14(3):145-54. http://dx.doi.org/10.32598/ijt.14.3.626.1.

45. El Shemy M, Azab N, Salim R. Zinc oxide nanoparticles: The hidden danger. Inter J Biochem Biophys Mol Biol 2017; 2(1):1-9. doi: 10.11648/j.ijbbmb.20170201.11.

46. Attia H, Nounou H, Shalaby M. Zinc oxide nanoparticles induced oxidative DNA damage, inflammation and apoptosis in rat's brain after oral exposure. Toxics 2018 ;6(2):29. https://doi.org/10.3390/toxics6020029.

47. Hegazy AA, Ahmed MM, Shehata MA, Abdelfattah MM. Changes in rats' liver structure induced by zinc oxide nanoparticles and the possible protective role of vitamin E. International Journal of Human Anatomy 2018;1(3):1. https://doi.org/10.14302/issn.2577-2279.ijha-18-2384.

48. Saliani M, Jalal R, Goharshadi K. Mechanism of oxidative stress involved in the toxicity of ZnO nanoparticles against eukaryotic cells. Nanomed J 2016; 3(1): 1-14. https://doi.org/10.7508/nmj.2016.01.001.

49. Shehata AS, Zidan RA, El-Mahroky SM, Abd El-Baset SA. Efficacy of platelet rich plasma on pancreatic injury induced by renal ischemia reperfusion in adult male rats. Ultrastructural Pathology 2022; 46(2):188-203. https://doi.org/10.1080/01913123.2022.204494.

50. Samah K, Aya A, Nafisa A, Reda H. Histological and Immunohistochemical Study of the Effect of Alendronate on the Submandibular Salivary Gland of Adult Male Albino Rat and the Possible Protective Effect of Propolis. The Medical Journal of Cairo University 2018;86 :3119-32. https://doi.org/10.21608/mjcu.2018.59886.

51. Badawi MS. A Study on the Antioxidant Activity of Rosmarinic Acid against Carbon Tetrachloride-Induced Liver Toxicity in Adult Male Albino Rats. International Journal of Morphology 2022; 40(1). http://dx.doi.org/10.4067/S0717-95022022000100157.

52. Logsdon CD, Ji B. The role of protein synthesis and digestive enzymes in acinar cell injury. Nature reviews Gastroenterology & hepatology 2013;10(6):362-70. https://doi.org/10.1038/nrgastro.2013.36.

53. El-Gamal DA, Ghafeer HH. Histological changes in adult rat pancreas upon chronic administration of aspartame. Egyptian Journal of Histology 2012 ;35(4):883-91. DOI: 10.1097/01.EHX.0000421550.95078.47.

54. Ding SP, Li JC, Jin C. A mouse model of severe acute pancreatitis induced with caerulein and lipopolysaccharide. World journal of gastroenterology 2003;9(3):584. https://doi.org/10.3748%2Fwjg.v9.i3.584.

55. Ismail ZO, Bhayana. V. Lipase or amylase for the diagnosis of acute pancratitis? Clin Biochem 2017; 50(18):1275-1280. https://doi.org/10.1016/j.clinbiochem.2017.07.003.

56. Ghadially FN. Ultrastructural pathology of the cell and matrix: a text and atlas of physiological and pathological alterations in the fine structure of cellular and extracellular components. 3rd ed. London: Butterworth-Heinemann; 2013. ISBN: 0407015701.

57. Wang L, Chen C, Guo L, Li Q, Ding H, Bi H, *et al*. Zinc oxide nanoparticles induce murine photoreceptor cell death via mitochondria-related signaling pathway. Artificial Cells, Nanomedicine, and Biotechnology 2018;46(sup1):1102-13. https://doi.org/10.1080/21691401.2018.1446018.

58. Han Z, Yan Q, Ge W, Liu ZG, Gurunathan S, De Felici M, *et al*. Cytotoxic effects of ZnO nanoparticles on mouse testicular cells. International journal of nanomedicine 2016;11:5187. https://doi.org/10.2147/IJN.S111447.

59. Khayal EE, Ibrahim HM, Shalaby AM, Alabiad MA, El-Sheikh AA. Combined lead and zinc oxide-nanoparticles induced thyroid toxicity through 8-OHdG oxidative stress-mediated inflammation, apoptosis, and Nrf2 activation in rats. Environmental Toxicology 2021; 36(12):2589-604. https://doi.org/10.1002/tox.23373.

60. Qin X, Zhang J, Wang B, Xu G, Yang X, Zou Z, *et al*. Ferritinophagy is involved in the zinc oxide nanoparticles-induced ferroptosis of vascular endothelial cells. Autophagy 2021;17(12):4266-85. https://doi.org/10.1080/15548627.2021.1911016

61. Cao C, Dai LI, Mu J, Wang X, Hong Y, Zhu C, *et al*. S1PR2 antagonist alleviates oxidative stress-enhanced brain endothelial permeability by attenuating p38 and Erk1/2-dependent cPLA2 phosphorylation. Cellular Signalling 2019; 53:151-61. https://doi.org/10.1016/j.cellsig.2018.09.019.

62. Hong XX, Wang HY, Yang JM, Lin BF, Min QQ, Liang YZ, *et al*. Systemic injury caused by taurocholate induced severe acute pancreatitis in rats. Experimental and Therapeutic Medicine 2022 ;24(1):1-2. https://doi.org/10.3892/etm.2022.11395.

63. Kumar V, Abbas AK, Fausto N, Aster JC. Robbins and Cotran pathologic basis of disease. 9th ed. Philadelphia: Saunders; 2014.

64. Somade OT, Ajayi BO, Olunaike OE, Jimoh LA. Hepatic oxidative stress, up-regulation of pro-inflammatory cytokines, apoptotic and oncogenic markers following 2-methoxyethanol administrations in rats. Biochemistry and biophysics reports 2020; 24:100806. https://doi.org/10.1016/j.bbrep.2020.100806.

65. Senapati VA, Kumar A, Gupta GS, Pandey AK, Dhawan A. ZnO nanoparticles induced inflammatory response and genotoxicity in human blood cells: A mechanistic approach. Food Chem. Toxicol 2015,85:61–70. https://doi.org/10.1016/j.fct.2015.06.018.

66. Wang B, Feng W, Wang M, *et al*. Acute toxicological impact of nano- and submicro-scaled zinc oxide powder on healthy adult mice. J Nanopart Res 2007;10(2):263–276. DOI:10.1007/s11051-007-9245-3.

67. Jancsó Z, Sahin-Tóth M. Chronic progression of cerulein-induced acute pancreatitis in trypsinogen mutant mice. Pancreatology 2022; 22(2):248-57. https://doi.org/10.1016/j.pan.2022.01.007.

68. Qiu YN, Wang GH, Zhou F, Hao JJ, Tian L, Guan LF, *et al*. PM2. 5 induces liver fibrosis via triggering ROS-mediated mitophagy. Ecotoxicology and Environmental Safety 2019 ;167:178-87. https://doi.org/10.1016/j.ecoenv.2018.08.050.

69. Peng YF, Lin H, Liu DC, Zhu XY, Huang N, Wei YX, *et al*. Heat shock protein 90 inhibitor ameliorates pancreatic fibrosis by degradation of transforming growth factor-β receptor. Cellular Signalling 2021; 84:110001. https://doi.org/10.1016/j.cellsig.2021.110001.

70. Genah S, Cialdai F, Ciccone V, Sereni E, Morbidelli L, Monici M. Effect of NIR Laser Therapy by MLS-MiS Source on Fibroblast Activation by Inflammatory Cytokines in Relation to Wound Healing. Biomedicines 2021;9(3):307. https://doi.org/10.3390/biomedicines9030307.

71. Spanehl L, Revskij D, Bannert K, Ehlers L, Jaster R. YAP activates pancreatic stellate cells and enhances pancreatic fibrosis. Hepatobiliary & Pancreatic Diseases International 2022. https://doi.org/10.1016/j.hbpd.2022.06.004.

72. Li Z, Lu D, Jin T, Liu X, Hao J. Nicotine facilitates pancreatic fibrosis by promoting activation of pancreatic stellate cells via α7nAChR-mediated JAK2/STAT3 signaling pathway in rats. Toxicology Letters 2021;349:84-91. https://doi.org/10.1016/j.toxlet.2021.06.012.

73. Yuan Y, Li Z, Li M, Jin T, Zhang X, Liu X, *et al*. Mitochondria oxidative stress mediated nicotine-promoted activation of pancreatic stellate cells by regulating mitochondrial dynamics. Toxicology in *Vitro* 2022 :105436. https://doi.org/10.1016/j.tiv.2022.105436.

74. Hu C, Yin L, Chen Z, Waldron RT, Lugea A, Lin Y, *et al*. The unique pancreatic stellate cell gene expression signatures are associated with the progression from acute to chronic pancreatitis. Computational and Structural Biotechnology Journal 2021 ;19:6375-85. https://doi.org/10.1016/j.csbj.2021.11.031.

75. Mohammadpour R, Dobrovolskaia MA, Cheney DL, Greish KF, Ghandehari H. Subchronic and chronic toxicity evaluation of inorganic nanoparticles for delivery applications. Advanced drug delivery reviews 2019;144:112-32. https://doi.org/10.1016/j.addr.2019.07.006.

76. Yousof SM, Erfan H, Hosny MM, Shehata SA, El-Sayed K. Subacute toxic effects of silver nanoparticles oral administration and withdrawal on the structure and function of adult Albino Rats' hepatic tissue. Saudi Journal of Biological Sciences 2022;29(5):3890-8. https://doi.org/10.1016/j.sjbs.2022.02.054.

77. Tang Y, Chen B, Hong W, Chen L, Yao L, Zhao Y, *et al*. ZnO nanoparticles induced male reproductive toxicity based on the effects on the endoplasmic reticulum stress signaling pathway. International Journal of Nanomedicine 2019;14:9563. https://doi.org/10.2147/IJN.S223318.

78. Chen R, Huo L, Shi X, Bai R, Zhang Z, Zhao Y, *et al*. Endoplasmic reticulum stress induced by zinc oxide nanoparticles is an earlier biomarker for nanotoxicological evaluation. ACS nano 2014;8(3):2562-74. https://doi.org/10.1021/nn406184r.

79. Sruthi S, Valappil Mohanan P. Engineered zinc oxide nanoparticles; biological interactions at the organ level. Current medicinal chemistry 2016;23(35):4057-68. https://doi.org/10.2174/092986732366616060724628.

80. Yang X, Shao H, Liu W, Gu W, Shu X, Mo Y, *et al*. Endoplasmic reticulum stress and oxidative stress are involved in ZnO nanoparticle-induced hepatotoxicity. Toxicology Letters 2015 ;234(1):40-9. https://doi.org/10.1016/j.toxlet.2015.02.004.

81. Murtaugh LC, Keefe MD. Regeneration and repair of the exocrine pancreas. Annu Rev Physiol 2015; 77:229-49. https://doi.org/10.1146/annurev-physiol-021014-071727.

82. Desai BM, Oliver-Krasinski J, De Leon DD, Farzad C, Hong N, Leach SD, *et al*. Preexisting pancreatic acinar cells contribute to acinar cell, but not islet β cell, regeneration. J Clin Invest 2007; 117(4):971-7. https://doi.org/10.1172%2FJCI29988.

83. Zhou Q, Melton DA. Pancreas regeneration. Nature 2018; 557(7705):351. https://www.cheric.org/research/tech/periodicals/doi.php?art_seq=1655319.

84. Frossard JL, Rubbia–Brandt L, Wallig MA, Benathan M, Ott T, Morel P, *et al*. Severe acute pancreatitis and reduced acinar cell apoptosis in the exocrine pancreas of mice deficient for the Cx32 gene. Gastroenterology 2003; 124(2):481-93. https://doi.org/10.1053/gast.2003.50052.

85. Barlass U, Dutta R, Cheema H, George J, Sareen A, Dixit A, *et al*. Morphine worsens the severity and prevents pancreatic regeneration in mouse models of acute pancreatitis. Gut 2018;67(4):600-2. http://dx.doi.org/10.1136/gutjnl-2017-313717.

الملخص العربى

تأثير جزيئات أكسيد الزنك متناهية الصغر وتأثيرإنسحابها على حويصلات البنكرياس فى ذكور الجرذان البيضاء البالغة: دراسة نسيجية و كيميائية حيوية وشكلية قياسية

ريهام سعيد أحمد محمود زغلول، مصطفى محمود أبوالعلا، صفاء جمعة تقى الدين، وسيلفيا كميل صديق ساويرس

قسم الهيستولوجيا وبيولوجيا الخلية ـ كلية الطب ـ جامعة الأسكندرية

مقدمة: تعد جزيئات أكسيد الزنك المتناهية الصغر واحدة بين أكثر الجزيئات المتناهية الصغر التي تستخدم على نطاق واسع في العديد من المجالات. كما أنها تستخدم في الوقت الحاضر بشكل متزايد في الغذاء كمادة حافظة. لذلك ، يصبح البشر أكثر عرضة لمخاطرها عن طريق الفم.

هدف البحث: يهدف البحث إلى تقييم تأثير الجرعات المختلفة من جزيئات أكسيد الزنك المتناهية الصغر على حويصلات البنكرياس وتأثيرإنسحابها.

المواد والطرق المستخدمة : تم تقسيم ثلاثون من ذكورالجرذان البيضاء البالغة بشكل عشوائى الى ثلاثة مجموعات متساوية. أعتبرت المجموعة الأولى مجموعة ضابطة. المجموعة الثانية) المجموعة المعالجة بواسطة جزيئات أكسيد الزنك المتناهية الصغر) تم تقسيمها الى مجموعتين فرعيتين تلقت كل منهما جزيئات أكسيد الزنك المتناهية الصغر بجرعات ١٠٠ و ٤٠٠ مج / كج من وزن الجسم/ يوم على التوالى لمدة ٢٨يوما عن طريق الفم. المجموعة الثالثة (مجموعة الإنسحاب) تم تقسيمها الى مجموعتين فرعيتين حصلتا على جزيئات أكسيد الزنك المتناهية الصغر كما هو موصوف سابقا في المجموعة الثانية ثم تركتا بلا علاج لمدة شهر. في الوقت المحدد ، تم جمع عينات الدم للتحليل الكيميائي الحيوي. بعد الذبح ، تم الحصول على أنسجة البنكرياس ومعالجتها لدراسات المجهرالضوئي و الإلكتروني. كما خضعت جميع البيانات المكتسبة للتحليل الإحصائي.

النتائج: أظهرت المجموعة المعالجة بـجزيئات أكسيد الزنك المتناهية الصغر تلفا في الخلايا المبطنة لحويصلات البنكرياس و الذي اعتمد على الجرعة. أظهرت الخلايا فجوات ، وخلخلة ، وشبكة إندوبلازمية خشنة متوسعة ، وتكاثف نووي ، وتنكس الميتوكوندريا الذي كان أكثر وضوحًا في الجرعة الأكبر. علاوة على ذلك ، أظهرت الدراسات البيوكيميائية ارتفاعًا ملحوظًا في مؤشرات البنكرياس وعوامل الأكسدة. كما أظهر التحليل الشكلي القياسي للعينات زيادة احصائية في نسبة مساحة ترسب الكولاجين. أدى انسحاب جزيئات أكسيد الزنك المتناهية الصغر من الجرذان المعالجة بـ ١٠٠ مج إلى تحسن ملحوظ في حويصلات البنكرياس بينما أظهرت النتائج تحسنا جزئيا في الجرذان المعالجة بـ ٤٠٠ مج.

الخلاصة: تسببت جزيئات أكسيد الزنك المتناهية الصغر في تغيرات نسيجيه ووظيفيه لحويصلات البنكرياس وهى تعتمد على الجرعة. هذه التغييرات تحسنت بعد إيقاف هذه الجزيئات المتناهية الصغر فى الجرعات الصغيرة بينما كان التحسن جزئيا بالنسبه للجرعة الأكبر.